Aliphatic polyesters for medical imaging and theranostic applications

Benjamin Nottelet, Vincent Darcos, Jean Coudane

Aliphatic polyesters for medical imaging and theranostic applications

Benjamin Nottelet *, Vincent Darcos, Jean Coudane

Institute of Biomolecules Max Mousseron (IBMM – CNRS UMR 5247), Department of Artificial Biopolymers, University of Montpellier, France

A B S T R A C T

Medical imaging is a cornerstone of modern medicine. In that context the development of innovative imaging systems combining biomaterials and contrast agents (CAs)/imaging probes (IPs) for improved diagnostic and theranostic applications focuses intense research efforts. In particular, the classical aliphatic (co)polyesters poly(lactide) (PLA), poly(lactide-*co*-glycolide) (PLGA) and poly(ε-caprolactone) (PCL), attract much attention due to their long track record in the medical field. This review aims therefore at providing a state-of-the-art of polyester-based imaging systems. In a first section a rapid description of the various imaging modalities, including magnetic resonance imaging (MRI), optical imaging, computed tomography (CT), ultrasound (US) and radionuclide imaging (SPECT, PET) will be given. Then, the two main strategies used to combine the CAs/IPs and the polyesters will be discussed. In more detail we will first present the strategies relying on CAs/IPs encapsulation in nanoparticles, micelles, dendrimers or capsules. We will then present chemical modifications of polyesters backbones and/or polyester surfaces to yield macromolecular imaging agents. Finally, opportunities offered by these innovative systems will be illustrated with some recent examples in the fields of cell labeling, diagnostic or theranostic applications and medical devices.

Keywords:
Medical imaging
Aliphatic polyesters
MRI
NIR
Micro and nanoparticles
Polymer micelles
Dendrimers
Diagnostic
Theranostic
Poly(lactide)

1. Introduction

Although molecular imaging was initially developed for clinical diagnostics and staging of human diseases, its strong impact on modern medicine practice recently led to the search for imaging probes (IPs) or contrast agents suited for more sophisticated applications including *in vivo* cell marking, early diagnosis of diseases, image-guided therapy or post-surgical medical devices follow-up [1,2].

To achieve a signal that is sufficient for clinical diagnostic purposes, and *a fortiori* for the more advanced applications, contrast agents (CAs) are generally required. The principle of CAs is to enhance visibility of specific tissues by increasing the signal to noise ratio (SNR) relative to surrounding tissues and therefore provide clear discrimination between normal and pathological regions in areas of interest [3]. As are therefore found in all molecular imaging modalities currently in use, namely magnetic resonance imaging (MRI), X-ray radiography/computed tomography (CT), ultra-sonography (US), optical imaging (bioluminescence and fluorescence), single photon emission computed tomography (SPECT) and positron emission tomography (PET), which will be discussed in more detail in the next section. To efficiently enhance SNR, CAs chemical structures are designed with respect to the imaging modalities characteristics. Historically, CAs were mostly low-molecular-weight compounds including atoms providing the expected signal modulation in the analyzed tissues (*i.e.*, gadolinium for MRI, iodine for X-ray, and radioactive atoms for PET and SPECT). However low-molecular-weight contrast agents generally face some severe limitations including, but not limited to, rapid diffusion from blood vessels into the interstitial space, toxicity or

Abbreviations: ATRP, atom transfer radical polymerization; CA, contrast agent; CT, computed tomography; CuAAC, copper-catalyzed azide–alkyne cycloaddition; DCA, dendritic contrast agent; D*h*, hydrodynamic diameter; DTPA, diethylene-triamine-pentaacetic acid; DOTA, 1,4,7,10-tetraazacyclododecane-1,4,7,10-tetraacetic acid; DOX, doxorubicin; EDC, ethyl(dimethylaminopropyl) carbodiimide; EDTA, ethylenediaminetetracetic acid; EGFR, epidermal growth factor receptor; FA, folic acid; Gd, gadolinium; HUVEC, human umbilical vein endothelial cells; IG, indocyanine green; IP, imaging probes; MCA, macromolecular contrast agents; MRI, magnetic resonance imaging; NHS, *N*-hydroxysuccinimide; NIR, near-infrared; NP, nanoparticles; OI, optical imaging; PAMAM, polyamidoamine; PBS, phosphate buffer saline; PCL, poly(ε-caprolactone); PEG, poly(ethylene glycol); PET, positron emission tomography; PGA, poly(glycolide); PGLA, poly(L-glutamic acid); PLA, poly(lactide); PLGA, poly(lactide-*co*-glycolide); PLL, poly(L-lysine); PTX, paclitaxel; QD, quantum dot; RES, reticuloendothelial system; RGD, arginine–glycine–aspartic acid tripeptide (cRGD, cyclic RGD); ROP, ring opening polymerization; scAb, single-chain antibody; SPECT, single photon emission computed tomography; SPION, super paramagnetic iron-oxide nanoparticles; TPGS, D-α-tocopherol polyethylene glycol succinate; UCA, ultrasound contrast agent; US, ultrasound; VEGF, vascular endothelial growth factor.

* Corresponding author.
E-mail address: benjamin.nottelet@univ-montp1.fr (B. Nottelet).

low sensitivity. In order to overcome these limitations, macromolecular imaging platforms raise increasing interest [4,5]. In fact, polymers offer an exciting toolbox in the frame of improved CAs development for advanced imaging applications. The large array of polymerization and functionalization techniques at the disposal of polymer chemists does not only provide fine control over the composition (hydrophilicity/hydrophobicity), the molecular weight, the size of the resulting self-assemblies, but also gives opportunity for biomolecules or targeting moieties attachment for a specific imaging of sites of interest in the body [2]. As a consequence, macromolecular contrast agents (MCAs) and polymeric carriers have gained interest for tuning the *in vivo* pharmacokinetic s/pharmacodynamics of the molecular IPs, as well as in the development of multimodal, multifunctional devices. One of the main applications is the use of polymeric systems for the high payload delivery of contrast agent to obtain clinically useful images, as low concentrations affect image quality [6]. Indeed, polymeric carriers able to carry high concentrations of CAs for the efficient and selective delivery of CAs into the selected tissues are proposed [7]. Among those carriers, micelles [4], dendrimers [8], or nanoparticles [9] have recently drawn much attention. Another growing field of investigations for MCAs and polymeric systems is the incorporation of the various combinations of imaging modalities, so called multimodal imaging, targeting ligands and therapeutic agents. Such multifunctional formulations designed for both diagnostic and therapeutic purposes are referred as "theranostics" [2,3]. This approach is a direct transposition of drug delivery concepts for the development of innovative medical imaging tools. Indeed, as drug carriers, nanoparticles (NPs) demonstrated over the past few decades their benefits in terms of drug stability increase, drug protection against degradation, site targeting and reduction of undesirable toxicity or side effects [10]. In that regard, the most common polymers used in drug delivery are the aliphatic polyesters poly(lactide) (PLA), poly(glycolide) (PGA), poly(ε-caprolactone) (PCL), and their copolymers, including the well-known poly(lactic-*co*-glycolic acid) (PLGA). This family of polymer has been a first choice for a variety of biomedical applications, ranging from surgical suture to drug eluting implants or drug nanocarriers [11,12]. This success story originated during the resorbable-polymer-boom of the 1970s and 1980s and is mostly due to their demonstrated biocompatibility and biodegradability that led to their validation by the regulatory agencies worldwide. Aliphatic polyesters and their copolymers are thermoplastics that present numerous advantages like tailorable degradation kinetics and mechanical properties, ease of shaping and manufacture, and whose broad spectrum of properties can easily be tuned for instance by the use of lactic acid-based stereocopolymers, or copolymerization with the biocompatible hydrophilic poly(ethylene glycol) (PEG) [13,14]. It is therefore not surprising to find them as core materials in the innovation pipeline of medical imaging strategies.

As a consequence, and although most classical and biostable polymeric materials have been reported for imaging applications, we will focus in this review on aliphatic polyesters as macromolecular imaging platforms. Following a first section dedicated to the imaging modalities in clinic, we will present the various approaches to associate the polymers and the IPs. These strategies are summarized in Scheme 1 with (i) particulate systems embedding IPs and contrast agents by physical encapsulation and without chemical modification of the polyesters (Section 3) and (ii) macromolecular contrast agents obtained by chemical ligation of CAs on the polymer backbones or on the surface of aliphatic polyester biomaterials (Section 4). In the last part, some advanced applications will be reviewed with examples in the field of cells trafficking, early diagnosis, theranostic and medical devices.

2. Imaging modalities

Molecular imaging is a non-invasive tool to visualize and characterize living organisms without perturbing them. The most common molecular imaging modalities are magnetic resonance imaging (MRI), optical imaging (fluorescence and bioluminescence), single photon emission computed tomography (SPECT), positron emission tomography (PET), computed tomography (CT), and ultrasound (US). A brief overview of these techniques will be discussed in this section and their main characteristics are summarized in Table 1.

2.1. Magnetic resonance imaging

Magnetic resonance imaging (MRI) is a non-ionizing technique that allows high spatial and temporal resolutions in clinical diagnosis and provides anatomical images of live subjects. MRI is typically used to enhance the detection and characterization of lesions within the body, define tissue boundaries or blood flow within regions of interest [15]. The basis for MRI signal is the precession of water hydrogen nuclei within an applied magnetic field where the relaxation process, through which the nuclei return to the original aligned state, can be exploited to produce an image [5,16]. To enhance the differentiation between tissues in MRI, contrast agents (CAs) are used to shorten the relaxation parameters (T1 and T2) of surrounding water molecules. The signal enhancement produced by MRI CAs (*i.e.* the efficiency of the CAs) depends on their longitudinal ($r1$) and transverse ($r2$) relaxivities (expressed in $mM^{-1}\ s^{-1}$), which is defined as the increase of the nuclear relaxation rate of water protons produced by 1 mmol per liter of CA. One can discriminate between negative CAs (T2 agents), that typically contain super paramagnetic species and induce the darkening of the contrast-enhanced tissue, or positive CAs (T1 agents), that typically contain paramagnetic elements and induce a brighter signal. T1 CAs are typically low molecular weight complexes of gadolinium (Gd^{3+} ion) that can be used as small molecules, conjugated to macromolecules, embedded in or grafted on nanoparticles [17]. On the opposite, T2 CAs are typically super paramagnetic iron-oxide nanoparticles (SPION) used as such or embedded in cargos [18]. Although MRI has good spatial resolution compared to other imaging modalities (e g. radionuclide or optical imaging), it suffers from low sensitivity. For this reason, large amounts of blood pool agents (BPA) currently approved for clinical uses (T1 CAs: Magnevist®, Dotarem®, Omniscan®; T2 CAs: Endorem®, Resovist®) are required to produce a detectable signal [19].

2.2. Optical imaging

Optical imaging is an emerging molecular imaging modality based on the detection of the photons emitted from fluorescent or bioluminescent probes. It presents a number of benefits over other imaging modalities including the cost, the high sensitivity of the signal detection, or the use of non-ionizing radiation. For example, fluorescence imaging has sensitivity similar to that of radionuclide imaging without the risk of radiation exposure. Unfortunately, the major drawback for clinical use is the poor deep tissue penetration (0–2 cm). Moreover, fluorescent optical imaging is prone to noise due to the tissue scattering of emitted photons in the visible area (390–600 nm). To circumvent these problems for *in vivo* imaging, the near-infrared (NIR) window (700–900 nm) is generally used with the advantages of reduced tissue scattering, and increased tissue penetration [20,21]. As a consequence, fluorescence imaging is currently one of the most common imaging techniques in preclinical use and molecular imaging is widely considered as the future for medical imaging in the clinical stage.

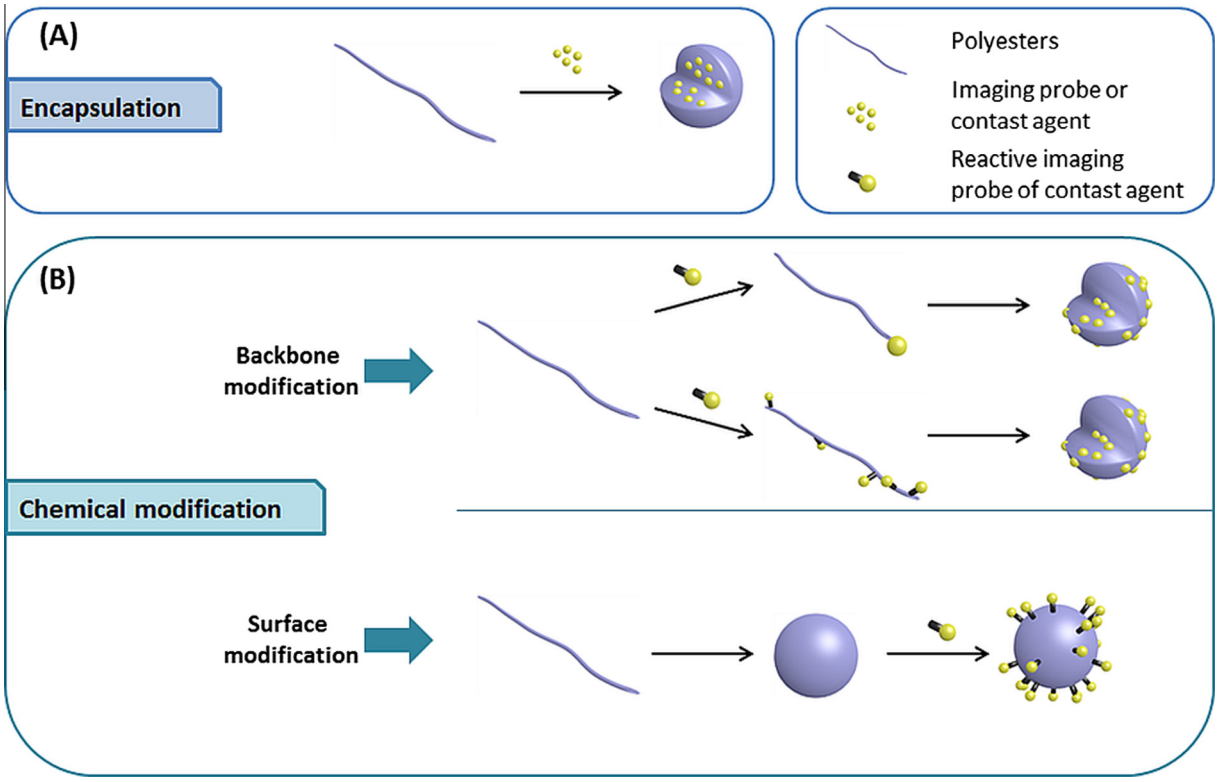

Scheme 1. Main strategies used to associate polymer and imaging probes or contrast agents with (a) nanoparticles embedding imaging probes and contrast agents by physical encapsulation and (b) macromolecular contrast agents obtained by chemical ligation of CAs on the polymer backbones or on the surface of aliphatic polyester biomaterials.

Table 1
Characteristics of imaging modalities.

Modality		Detection	Imaging probes	Advantage	Disadvantage	Clinical application
Magnetic resonance imaging (MRI)		Magnetic field and radio-wave	Gadolinium Iron oxide Manganese oxide	Non-invasive technique Non-ionizing technique High spatial resolution No tissue penetration limit	Relatively low sensitivity Long scan times High cost	Yes
Optical imaging (OI)		Fluorescence or Bioluminescence	Fluorescent probes Bioluminescent probes	Non-invasive technique Non-ionizing technique High sensitivity	Relatively low spatial resolution Poor tissue penetration	Under development
X-ray and computed tomography (CT)		X-ray	Gold nanoparticles Iodine	Non-invasive technique High spatial resolution No tissue penetration limit	Radiation risk High dose of ionizing radiation	Yes
Ultrasound (US)		Ultrasonic waves	Microbubbles	Non-invasive technique Non-ionizing technique Real-time Low cost	Relatively low spatial resolution Poor contrast Operator dependent analysis	Yes
Radionuclide imaging	SPECT imaging	γ-ray	^{18}F, ^{64}Cu, ^{11}C, ^{15}O	High sensitivity No tissue penetration limit Quantitative result	Radiation risk Low spatial resolution	Yes
	PET imaging	γ-ray	^{99m}Tc, ^{111}In	High sensitivity No tissue penetration limit Quantitative result	Radiation risk Low spatial resolution High cost	Yes

2.3. X-ray and computed tomography (CT)

X-ray imaging is a low cost imaging technique that has been used for over a century for medical imaging following X-rays discovery by Roentgen in 1895. In the early 1970s, X-ray computed tomography (CT) was developed to produce cross-sectional images of the body. The mechanism of CT imaging is based on the absorption of X-rays as they pass through tissues with distinct degrees of attenuation that depend on the atomic number and electron density of the tissues [22]. These differences in absorption between bone, fat, water, and air yield high contrast images of anatomical structures. Low molecular weight CT CAs or radio-opacifying agents are therefore typically used to increase attenuation, including gold nanoparticles, heavy metal powders (tantalum), inorganic salts of heavy elements (barium sulfate, bismuth sulfide), or organic compounds containing a heavy atom (triiodosubstituted aromatic compounds) [23–25]. In particular, iodinated CAs permit assessment of ventricular volumes, vascular structures, etc. Advantageously, no limit on tissue penetration depth is observed and a good spatial resolution is obtained. Small-molecular CAs are however characterized by rapid extravasation and clearance. In addition, they can induce well-known recurrent problems like acute renal toxicity or adverse allergic and pseudo-allergic reactions [23,26] which, in addition to ionizing character of X-ray, explains that X-ray imaging still represents today only ca. 7% of the medical images done. However, a renewed strong interest is currently witnessed, mainly due to the development of micro-computed tomography (micro-CT) application to soft tissues, where specific X-ray CAs having a selective biodistribution have been designed [27,28].

2.4. Ultrasound

Ultrasound (US) is probably the most common molecular imaging modality used in clinics. The reasons are the low cost, the simplicity, the real-time imaging, and the safety of this technique [29]. US images are obtained based on the sound wave reflected back from the internal organs. Sound waves are emitted from a transducer placed against the skin, and the reflected signal is detected and used to make an image. However, this modality suffers from poor resolution and contrast. Moreover, ultrasound imaging is an operator dependent method, reducing the reproducibility. Like for other modalities, contrast can be improved by introducing a material with different acoustic properties from that of tissues. Optimal density differences are obtained when the CA is a gas, because tissues are primarily composed of liquid. Therefore most ultrasound CAs are microbubbles formulations (microspheres with porous or hollow inner structure with a diameter of 1–10 μm) that circulate in the intravascular compartment [29,30].

2.5. Radionuclide imaging

Nuclear molecular imaging, such as SPECT and PET, is one of the most common techniques used in clinics. Both modalities are based on γ-ray emissions, radiopharmaceuticals are administered and can be detected. Compare to optical imaging, no limit on tissue penetration depth is observed with SPECT and PET. Radiopharmaceuticals are used as tracers with high detection sensitivity. Thus, whole-body imaging is possible. Moreover, SPECT and PET are quantitative methods, which is an advantage compared to MRI and optical imaging. Nowadays, SPECT is more widely used than PET, indeed SPECT radiopharmaceuticals are easy to synthesize with longer half-life than PET radiopharmaceuticals. After all, the main drawback of these modalities is the exposure to nuclear radiation. Indeed, it is interesting to note that radiopharmaceuticals can be also administrated for radiotherapy [31,32].

3. Polyesters embedding imaging probes

The entrapment of CA in a particulate system allows getting a high concentration of contrast agent at the imaging site. Advantageously, it also makes possible to overcome some of the main limitations of current low molecular weights CAs, including rapid clearance, non-specific distribution or toxicity. This approach has therefore been developed for all imaging modalities based on the classical encapsulating strategies using nanoparticles, micelles, dendrimers, etc. (Scheme 1A). In addition, as countless therapeutic approaches rely on drug loading in polyesters assemblies, the simultaneous entrapment of both CAs and drugs in a single polyester-based system is very straightforward and appealing in the frame of theranostic tools development. The following aims at reporting the various approaches that have been proposed for the preparation of aliphatic polyesters particulate systems for imaging or theranostic.

3.1. MRI modality

As discussed in Section 2, although MRI has good spatial resolution it suffers from low sensitivity. For this reason, large amounts of CAs are required to produce a detectable signal for clinical uses [19]. For example Gd-chelates of diethylene-triamine-pentaacetic acid (DTPA), or other derivatives like 1,4,7,10-tetraazacyclododecane-1,4,7,10-tetraacetic acid (DOTA), are used at a recommended dose of 0.1 mmol/kg, and distribute broadly into tissues before clearance through kidneys. However, the administration of repeated high doses of these contrast agents may lead to concerns over accumulation and potential toxicity. It is known that Gd complexes can be responsible for nephrogenic systemic fibrosis disorder (NFS) in patients with existing renal failure [33,34]. The same concerns were raised for the SPION-based CAs used in current MRI procedure, like Resovist® (Dextran-coated SPION), due to their accumulation in the visceral organs. In addition, low molecular weight CAs have limits *in vivo* with rapid elimination restricting timing for studies and extravasation out of the vasculature reducing contrast from surrounding tissue in the frame of angiography or to tissue perfusion evaluation [5]. To get high payload and decreased toxicity, various polyester-based systems have been proposed and are discussed in the following (Table 2).

3.1.1. SPION-based systems

3.1.1.1. Micro- and nanoparticles. Based on the long track record of PLGA nanoparticles in the field of drug delivery, encapsulation of magnetic nanoparticles of Fe_3O_4 (magnetite) in PLGA nanoparticles or microparticles has been extensively used in the recent years to produce theranostic tools with MRI imaging capabilities [18,73–81]. Lee et al. were among the first to prepare PLGA NPs containing super paramagnetic iron-oxide nanoparticles (SPION) by using an emulsification–diffusion method to generate contrast agents to be used in kidneys of rabbit [35]. As an alternative to SPION, MnO nanocrystals have also been entrapped in PLGA NPs at high loadings (50 wt%) [36]. In this case, following endocytosis into low pH compartments within the cells, the particles eroded and MnO dissolved to release Mn^{2+} that caused the cells to appear bright on MR images. Hydrophobic SPION/PLGA nanoparticles need however to be stabilized by a hydrophilic dispersant in aqueous solution which may be cytotoxic and not degradable. To make the NPs formulations more stable, less sensitive to aggregation, as well as to avoid RES uptake and reduce side effects, other formulation alternatives were considered. Coating of NPs with approved surfactants, for example Polysorbate 80, was proposed [82]. For stability reasons, covalently hydrophilized NPs are however generally preferred over surface physically absorbed stabilizers. Wang

Table 2
Particulates systems based on aliphatic polyesters for MRI.

Contrast agent	Type	(Co)polyester	Relaxivity ($mM^{-1}\ s^{-1}$)		Average size (D*h*, nm)	Targeting moiety	Additional comments	Refs.
			*r*1	*r*2				
SPION	Nanoparticles	PLGA	–	–	120	–	–	[35]
		PLGA	–	–	140	–	MnO nanocrystals	[36]
		PEG-*b*-PLGA	–	532	230	–		[37]
		PLGA-*b*-PEG-*b*-PLGA	–	14	–	–	Dual imaging OI	[38]
		PEG-*b*-PLA	–	220–250	140–170	–	–	[39]
		TPGS-*b*-PLA	–	165	250	–	Dual imaging QD	[40,41]
		PEOz-*b*-PLA	–	12	180	FA	PTX	[38]
		PLGA + chitosan	–	180	270	–	ξ = 28 mV	[42]
		PLGA + PEG polymersome	–	–	485	FA	DOX; ξ = 43 mV	[43]
		P(LA-*co*-MA)	–	165	100		ξ = −35 mV	[44]
		PLGA + poly(allylamine hydrochloride)/PEG	–	–	–	scAb antibody	Docetaxel	[45]
		Dextran-*g*-PCL	–	–	–		–	[46]
		PEG-*b*-PPSu-*b*-PEG	–	–	250		PTX	[47]
		mPEG-*b*-various polyesters	–		10		Coating	[48]
	Micelles	PEG-*b*-PCL	–	60–170	35–110	FA		[8,49,50]
		PEG-*b*-PCL	–	270	–		Mn-SPION	[51]
		PCL-*b*-PAA	–	215	100			[52]
		P(NIPAAm-*co*-AAm)-b-PCL	–	97	70		DOX; thermo-responsive	[53]
		PEG-*b*-PLA	–	360	60			[54]
		PEG-*b*-PLA	–	–	46	cRGD	DOX	[55]
		PEG-*b*-PLA-*b*-PEG-acrylate	–	222	23 × (100–200)	FA	DOX; wormlike micelles	[56]
	Micro- & nanocapsules	PLA	–	–	2000–8000	–	–	[57,58]
		PEG-*b*-PLA	–	–	–	–	–	[59]
Gd-chelate	Microparticles	PLGA	–	–	4800	–	VEGF	[60]
		PLA and PEG-*b*-PLA	–	–	900–1800	–	Dual imaging Fluo, US	[61,62]
	Nanoparticles	PEG-*b*-PLA	–	–	190	–	–	[63]
		PLGA	≈18	–	155	–	Lipophilic chelate	[64]
	Polymersomes	PEG-*b*-PBu and PEG-*b*-PCL	7.5	–	130	–	–	[65]
		PEG-*b*-PLGA	2.8	–	280	–	DOX	[66]
	Microcapsules	PLGA	–	–	1500	–	Dual imaging US	[67]
Gd oxide	Nanoparticles	PLGA	1.9	8.4	–	–	–	[68]
Perfluorocarbons	Nanoparticles	PLGA	–	–	–	–	F-19 MRI	[69]
	Nanocapsules	PEG-*b*-PLGA	–	–	120	RGD	F-19 MRI	[70,71]

Note: Dotarem® *r*1 = 3.5 $mM^{-1}\ s^{-1}$; Magnevist *r*1 = 3.8 $mM^{-1}\ s^{-1}$ [5]/Resovist *r*2 = 151 $mM^{-1}\ s^{-1}$; Feridex® *r*2 = 98 $mM^{-1}\ s^{-1}$ [72]; (–) not applicable or information not provided.

et al. proposed the use of PEG_{2k}-*b*-$PLGA_{30-50k}$ instead of PLGA to generate nanoparticles [37]. Their PEG-*b*-PLGA NPs formulation achieved ca. 35% less cytotoxicity in comparison with the Resovist® after 48 h incubation at the same Fe concentration. Relaxivity was also higher, with *r*2 = 532 $mM^{-1}\ s^{-1}$ for the PEG-*b*-PLGA. Triphenylamine-PLGA-*b*-PEG-*b*-PLGA triblock was also considered for dual modality imaging with a relaxivity of *r*2 = 14 $mM^{-1}\ s^{-1}$ and a maximal emission wavelength at λ = 453 nm [38]. Other authors used PLA instead of PLGA. For example PEG_{2k}-*b*-PLA_{5k} formed stable NPs with 140–170 nm average diameters and up to 12 wt% SPION loading and relaxivity *r*2 = 220–250 $mM^{-1}\ s^{-1}$ as compared to *r*2 = 72 $mM^{-1}\ s^{-1}$ and *r*2 = 105 $mM^{-1}\ s^{-1}$, for Feridex® and Endorem® respectively [39].

Copolymer made of poly(lactide) (PLA) and D-α-tocopherol polyethylene glycol succinate (TPGS) was also proposed for lowering the side effects. The SPION-loaded $TPGS_{1k}$-*b*-PLA_{12k} NPs were prepared by the single emulsion method (0.5 wt% Fe) or the nanoprecipitation method (1.3 wt% Fe) (Fig. 1A). The latter had a relaxivity of *r*2 = 165 $mM^{-1}\ s^{-1}$ and formulation at the clinically approved dose of 0.8 mg Fe/kg could be cleared within 24 h in comparison with several weeks for Resovist® while being less toxic toward NIH-3T3 mouse fibroblast cells [40]. The system was further improved by association with quantum dots for dual modality imaging [41]. Although PEG is the most commonly hydrophilic block, polyoxazoline has also been considered as an alternative. Folate-poly(2-ethyl-2oxazoline)-*b*-poly(D,L-lactide) (FA-PEOz-*b*-PLA) was proposed for the coencapsulation of SPION and PTX. 30%-FA-NP with a mean diameter of 180 nm and *r*2 = 12 $mM^{-1}\ s^{-1}$ were obtained and injected to HeLa-bearing mice. At PTX concentrations of 5 mg kg^{-1}, reduction in tumor volume at day 23 was 50% for the 30%-FA-NP compared to 21% for free PTX, whereas significantly lower T2 signal intensities at the tumor site was obtained [38].

Beside these non-ionic NPs, charged NPs have also been described. It includes NPs with PLGA core and a positively-charged glycol chitosan shell to avoid NPs aggregations [42,83]. The resulting NPs had a positive zeta potential (ξ = 28 mV) and a relaxivity *r*2 = 180 $mM^{-1}\ s^{-1}$ with respect to Fe. Once taken up by the liver RES Kupffer cells, NPs allowed liver imaging over a 4 weeks period [42]. In a similar approach, Wang et al. prepared DOX and SPION embedding PLGA nanoparticles that were coated with folate-PEG conjugated polymersome shells composed of octadecyl-quaternized lysine modified chitosan (OQLCS) conjugated to FA or PEG (ξ = 43 mV) [43]. Anionic counterparts were also prepared from poly(DL-lactic acid-*co*-α,β-malic acid) low molecular weights polycondensates (*Mn* < 2.5 kDa) that yielded NPs with an anionic surface (ξ = −35 mV) and *r*2 = 165 $mM^{-1}\ s^{-1}$ [44]. Advantage was also taken from layer-by-layer self-assemblies to functionalize the surface of SPION embedding NPs. Gao et al. prepared core–shell structures with PLGA core embedding SPION

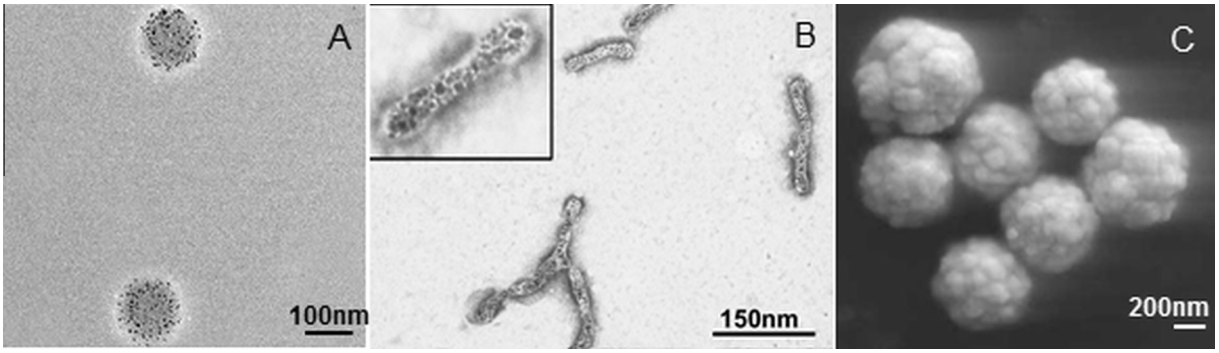

Fig. 1. Examples of nanoparticles and micelles with MRI capacities. (A) TEM images of PLA-TPGS/SPION nanoparticles (adapted with permission from Prashant et al. [40]); (B) SPION/DOX-loaded wormlike polymer vesicles with crosslinked inner PEG layers, formed by the triblock copolymers (adapted with permission from Yang et al. [56]) and (C) SEM image of the W/O/O particles with encapsulated rhodamine and a silver cage on the exterior of the particle (adapted with permission from Doiron et al. [62]).

(5 wt%) and docetaxel (5 wt%), associated with a poly(allylamine hydrochloride)/scAB-poly(ethylene glycol)–COOH shell, where scAb provided targeted delivery to prostate stem cell antigen-positive cancer cells [45]. The resulting constructs were injected in nude mice bearing PC3M xenografts and provided MRI negative contrast enhancement, as well as decreased tumor growth during the 76-day study duration.

Although PLGA and PLA are largely used for SPION encapsulation, other polyester-based copolymers have also been proposed. PCL microparticles embedding SPION were obtained by emulsification–diffusion method. High SPION encapsulation efficacy (>90%) was obtained yielding a magnetite loading of up to 30 wt% in particles having a diameter in the range 5–15 μm [84]. Alternatively, amphiphilic dextran-*g*-PCL copolymer, prepared by ROP of ε-caprolactone from silylated dextran, was also used [46]. Triblock copolymers of PEG and poly(propylene succinate) (PEG_{2k}-*b*-$PPSu_{6-19k}$-*b*-PEG_{2k}) were used to generate taxol (ca. 5–8 wt%) and SPION loaded NPs [47]. Diblock $mPEG_{2-5k}$-*b*-$polyesters_{5k}$, where the polyester block was prepared by polycondensation of various diols (ethylene glycol or 1,6-hexanediol) and diacids (malonic or maleic acid), were also synthesized and used as coating to stabilize SPION in water. Small NPs (D*h* ≈ 10 nm) containing up to 37 wt% of Fe_3O_4 were produced and used to encapsulate indomethacin as a model drug [48].

3.1.1.2. Micelles. Superparamagnetic polymeric micelles of PEG_{5k}-*b*-PCL_{5k} were proposed by Ai et al. [49] as an alternative to dextran matrices for the encapsulation of SPION. Micelles had diameters ranging from D*h* ≈ 75–110 nm as a function of the SPION size (4–16 nm) and loadings of magnetite were up to 54%. High relaxivity ($r2$ = 170 Fe mM^{-1} s^{-1}) was found compared to Resovist® allowing detection limits at 5 μg/mL of loaded micelles, which corresponds to a micelle concentration of 5 nM. In further development, FA-PEG_{4k}-*b*-PCL_{1-7k} micelles (D*h* ≈ 35 nm) were evaluated *in vivo* for tumor targeting [50,85]. Prolonged circulation and slower liver accumulation were achieved with the micelles that were able to encapsulate up to 35 wt% SPION ($r2$ = 58 Fe mM^{-1} s^{-1}). A similar approach was reported by Lu et al. with the same polymer but with Mn–SPION ($r2$ = 270 Mn + Fe mM^{-1} s^{-1}). Time window for enhanced-MRI of 36 h with obvious contrast on liver image was reported [51].

Like for the nanoparticles, alternative to PEG hydrophilic block can be found. For example partly degradable poly(ε-caprolactone)$_{11k}$-*b*-poly(acrylic acid)$_{2.5k}$, was synthesized via ring-opening polymerization (ROP) of ε-caprolactone followed by ATRP of *tert*-butyl acrylate. Micelles embedding SPION were obtained and stabilized via surface crosslinking of an inorganic silica layer prior to surface pegylation [52]. Crosslinked micelles exhibited an average diameter and a mean thickness of silica crosslinking layer around 100 nm and 10 nm, respectively, whereas their relaxivity was equal to $r2$ = 215 mM^{-1} s^{-1}. Thermo-responsive micelles prepared from poly(*N*-isopropylacrylamide-*co*-acrylamide)-*b*-poly(ε-caprolactone) copolymer (*Mn* = 14 kDa) were used to encapsulate both SPION and DOX, whereas their surface was functionalized by integrin β4 antibody to target squamous cell carcinoma of the head and neck. These micelles were proposed as magnetic hyperthermia-mediated drug release and imaging agents ($r2$ = 97 mM^{-1} s^{-1}). P(NIPAAm-*co*-AAm) was chosen to adjust the LCST of the copolymer to 43 °C and therefore gain stability at physiological temperature whereas triggering drug release at higher temperature [53].

PLA-based micelles have also been employed to encapsulate SPION. PEG_{5k}-*b*-$PLA_{2.5k}$ block copolymers were prepared and used for the preparation of NPs with SPION loading of ca. 55% and relaxivity $r2$ = 360 mM^{-1} s^{-1} [54]. Nasongkla et al. employed amphiphilic block copolymers of PEG_{3k}-*b*-PLA_{4k} bearing cRGD moieties to prepare SPION–DOX-loaded polymer micelles (SPION loading 7 wt%) as a tumor-targeting, MRI drug delivery system [55]. To enhance drug loading level and flexibility over spherical micelles original wormlike micelles used for dual MRI imaging and DOX release were reported by Yang et al. who used heterobifunctional amphiphilic triblock copolymers FA-PEG_{5k}-PLA_{21k}-PEG_{2k}-acrylate (Fig. 1B) [56]. The long FA–PEG segments were mostly segregated to the outer hydrophilic PEG layers of the wormlike vesicles providing active tumor-targeting ability, while the short PEG-acrylate segments were segregated onto the inner hydrophilic PEG layers of the vesicles, thereby allowing the inner PEG layers to be crosslinked for enhanced *in vivo* stability. The average diameter of the wormlike vesicles was about 23 nm, and the length was between 100 and 200 nm. SPION loading was 48 wt% allowing twice higher relaxivity for the SPION/DOX-loaded micelles ($r2$ = 222 Fe mM^{-1} s^{-1}) compared to Feridex®.

3.1.1.3. Micro- and nanocapsules. PLA microbubbles containing Fe_3O_4 nanoparticles were prepared for dual imaging modalities, namely MRI and ultrasound [58]. The diameter of microbubbles was controlled by the formulation conditions, resulting in particles with diameters in the range 2–8 μm. In further development, it was demonstrated that improved T2-weighted MRI capabilities were obtained with SPION in the shell rather than in the inner cavity of the microbubbles with a 50% increase of relaxivity $r2$ [57]. Xu et al. pushed this approach one step further thanks to PEG-*b*-PLA (*Mw* = 20 kDa, EG/LA = 1:9, wt%) nanocapsules obtained by the combination of double emulsification with the interfacial coprecipitation synthesis of Fe_3O_4 nanoparticles. These nanocapsules embedded up to 40 wt% SPION [59].

3.1.2. Gadolinium-based systems

3.1.2.1. Micro- and nanoparticles. NP embedding Gd complexes have been proposed for monitoring drug delivery vehicles non-invasively with MRI. Faranesh et al. were among the first to propose PLGA microspheres containing VEGF and Gd-DTPA complex. PLGA microspheres had a mean diameter of 48 μm with gadolinium loading of 17 μg/mg and could be used for sustained release of VEGF over a 6 week period [60]. Other authors prepared $PLGA_{11k}$ or $PEG_{3.5k}$-*b*-PLA_{52k} microparticles embedding up to 30 wt% Gd-DTPA for atherosclerosis plaque detection [61]. MRI CA was encapsulated by a water-in-oil-in-oil double emulsion solvent evaporation technique to yield microparticles with mean diameters between 0.9 μm and 1.8 μm. Loaded particles showed minimal cytotoxic effects when HUVEC were exposed to high concentrations of particles, while relaxivity similar to the one of free Gd-DTPA was obtained. This platform was further used for dual modality imaging (optical/MRI or US/MRI) by encapsulation of Rhodamin and/or precipitation of silver nanocage around the particles (Fig. 1C) [62].

In a similar but downscaling approach, Chen et al. reported on the preparation of PEG_{4k}-*b*-PLA_{48k} nanoparticles that were co-incubated with Gd-DTPA that absorbed at the surface [63]. *In vivo* injection of nanoparticles in rats showed a slower increase of MRI signal compared to that of free Gd-DTPA with improved imaging window (*i.e.*, in liver 4 h against less than 10 min). The disadvantage of the incorporation of these hydrophilic compounds was however their fast release from the particle (few hours) with a marked difference in the biodistribution and clearance with respect to the intact particle. To both improve relaxivity and retention of Gd chelate in the particles, the incorporation of amphiphilic or lipophilic Gd chelate in PLGA nanoparticles was recently explored [64,86]. For example lipophilic Gd chelate (Gd-DOTA-C12) was incorporated in PEGylated PLGA nanoparticles at high Gd loading (1.1×10^4 Gd centers per nanoparticle). The resulting NPs exhibited a relaxivity up to sixfold greater than DOTAREM®. This increase was explained by the nanoparticle framework that constrained the lipophilic Gd chelate motion and favorably impacted the Gd chelate rotational correlation time [64].

3.1.2.2. Polymersomes. An original approach based on polymersomes was reported by Cheng et al. [65]. Although aliphatic polyesters were not present in the final structure, the ability of PCL to degrade was exploited to yield porous polymersomes with improved relaxivity. Polymersomes with permeable membrane were produced through the aqueous assembly of the PEG-*b*-poly(butadiene) ($PEG_{1.3k}$-*b*-$PBu_{2.5k}$) and PEG_{2k}-*b*-$PCL_{2.7k}$, followed by the hydrolysis of PCL blocks. To prevent the leakage of Gd-DTPA through the pores, Gd-DPTA was conjugated to polyamidoamine (PAMAM) dendrimers prior to encapsulation. As a result of the slower rotational correlation time of Gd-labeled dendrimers and the porous outer membrane of the nanovesicle a relaxivity $r1 = 7.5\ mM^{-1}\ s^{-1}$ per Gd was measured, which represents a 4.4-fold improvement compared with nonporous vesicles with encapsulated Gd-DTPA. The same strategy was recently followed by Liu et al. who replaced the encapsulated DCAs by bovine serum albumin–gadolinium (BSA–Gd) complexes and used PEG_{5k}-*b*-$PLGA_{5k}$ for the polymersomes formulation. Finally, DOX was also loaded in the PLGA inner layer of the polymersome membranes (≈20 wt%) to yield theranostic tools ($r1 = 2.8\ mM^{-1}\ s^{-1}$ per Gd) (Fig. 2A) [66].

3.1.2.3. Micro- and nanocapsules. Similarly to SPION, Gd-DTPA has also been incorporated in microbubbles for dual imaging. Ao et al. prepared Gd-DTPA fluorocarbon-filled PLGA microbubbles by using double emulsion method. The microbubbles were spherical in shape with mean diameter of ca. 1.5 μm and a Gd loading of

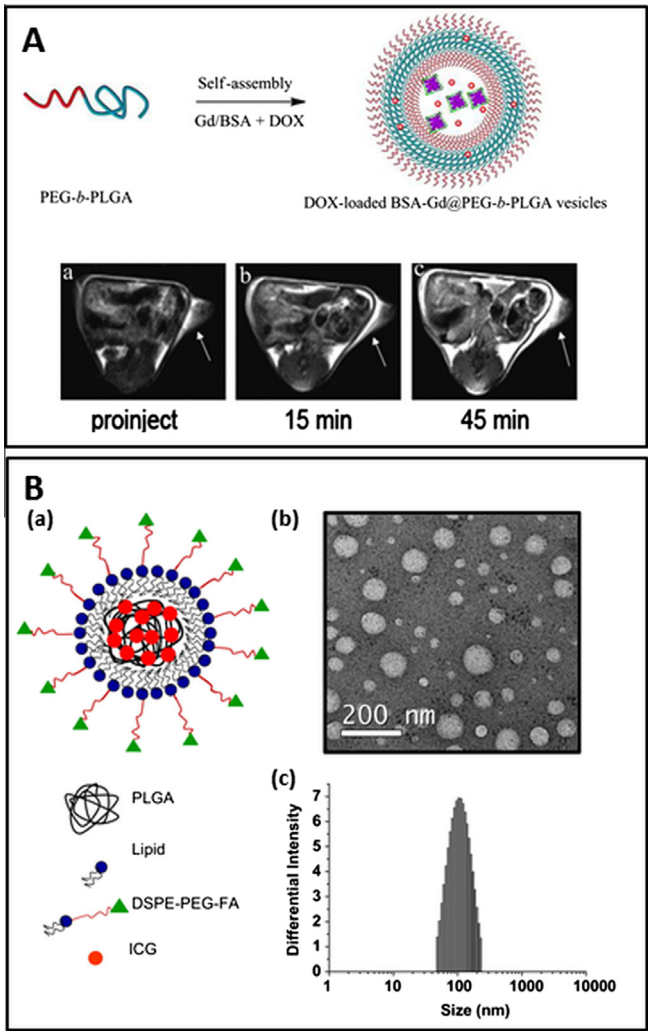

Fig. 2. Examples of polymersomes and liposomes with imaging capacities. (A) Self-assembly of PEG-*b*-PLAGA with bovine serum albumin gadolinium (top row) and T1-weighted MR images of the nude mice acquired (a) prior to and (b and c) post-injection of BSA-Gd@PEG-b-PLGA vesicle suspension at different times (bottom row). The white arrows denote xenograft tumors (adapted with permission from Liu et al. [66]). (B) (a) Self-assembly of tumor targeting NIR probe (FA-ICG-PLGA-lipid NPs) for NIR molecular imaging, (b) TEM image of FA-ICG-PLGA-lipid NPs and (c) size distribution of FA-ICG-PLGA-lipid NPs by dynamic light scattering (reprinted with permission from Zheng et al. [87]).

25 μg/mg. They were used for *in vivo* imaging of hepatic vessels and the liver parenchyma of rabbits [67].

3.1.2.4. Miscellaneous approaches. An original approach has been reported by Sitharaman et al. who used Gd^{3+} ions-doped ultra-short single-walled carbon nanotube (gadonanotubes with 3 wt% Gd, $r2 = 578\ mM^{-1}\ s^{-1}$, $r1 = 170\ mM^{-1}\ s^{-1}$), to prepare gadonanotubes-reinforced PLGA nanocomposites (2 wt% gadonanotubes) [88]. Enhanced MRI contrast was observed *in vitro*, however, like for Gd-DPTA chelates, a release of nanotubes after few days was noticed yielding to a loss of MRI visibility. Another original approach for MRI-based cell tracking used gadolinium oxide (Gd_2O_3) based contrast agents instead of Gd-chelates. Gd_2O_3 nanocrystals were encapsulated within PLGA nanoparticles with $r1 = 1.9\ mM^{-1}\ s^{-1}$ and $r2 = 8.4\ mM^{-1}\ s^{-1}$ [68]. For F-19 MRI modality, large fluorocarbons labeling compounds that are insoluble in aqueous environments have been encapsulated in PLGA NPs. Loadings up to 0.4 mg/mg PLGA were obtained thus allowing MR imaging in mice over a 7-day period [69]. $PLGA_{22k}$-PEG_{5k}

nanocapsules containing a liquid core of perfluorooctyl bromide were also synthesized as contrast agents for F-19 MRI. The nanocapsules demonstrated improved circulation time with accumulation in CT26 xenograft tumor 7 h after administration to mice, whereas plain nanocapsules remained undetectable [71]. In an incremental work, the same group studied the influence of RGD functionalization of the nanocapsules on their accumulation in the tumors but could not demonstrate improved accumulation compared to the PEGylated nanocapsules [89].

3.2. Optical imaging modality

During the last decade, fluorescent dye-encapsulating polymer nanoparticles have been paid growing attention for potential applications in optical imaging. Nevertheless, to the best of our knowledge only two fluorophores (indocyanine green and fluorescein) are currently approved by the Food and Drug administration for medical use. For instance, the well-known fluorophore rhodamine B was approved for use in 1966 but was subsequently proscribed [90]. Indeed, the toxicity of the wide range of organic dyes bearing aromatic rings is not well-known. Moreover, most of the organic dyes are unstable and quickly cleared from the body through the kidneys. To overcome these problems of toxicity and instability, an interesting solution is to encapsulate the dye into the degradable nanoparticle. Although optical imaging with conventional fluorescent dyes such as anthracene, pyrene, coumarin suffers from important limitations (low quantum yield, photobleaching etc.), one of the first examples described by Panyam et al. reported degradable nanoparticles loaded with the 6-coumarin [91]. The degradable nanoparticles were prepared from PLGA. The authors concluded that 6-coumarin could serve as a useful fluorescence probe to study the cellular distribution of the NPs. To target the delivery of NPs in the cytoplasm, PLGA was conjugated with fluorescein and biotin [92]. After *in vivo* administration of the PLGA NPs, *in vivo* distribution of the NPs both in brain areas and in liver parenchyma was carried out using optical imaging. Then, different examples of fluorescent dyes encapsulated into PLGA NPs have been reported [62,93–95].

With the development of near infrared (NIR) fluorescence optical imaging for *in vivo* experiments, new fluorescent probes with fluorescence in the NIR spectrum (700–900 nm) were investigated. As mentioned previously, the NIR area is most appropriate for *in vivo* imaging than visible area. Indeed, the NIR fluorescence probe has quite low tissue absorption, minimum autofluorescence, which induces a higher tissue penetration than visible optical probe for *in vivo* imaging application. Indocyanine green (ICG)-loaded biodegradable NPs were reported by Zheng et al. for *in vivo* imaging application [87,96]. ICG is the only NIR probe that has been approved by the FDA. But, ICG suffers from its poor aqueous stability, concentration-dependent aggregation, rapid elimination from the body, and lack of target specificity. To overcome these limitations, ICG-loaded PLGA nanoparticles bearing a targeting ligand folic acid (FA-ICG-PLGA-lipid NPs) were prepared by a single-step self-assembly and nanoprecipitation method (Fig. 2B). TEM image revealed that the NPs were dispersed as individual NPs with a well-defined spherical shape and homogeneously distributed with an average hydrodynamic diameter of 102 nm.

To protect the NIR probes and stabilize the NPs, amphiphilic copolymer micelles were used. Moreover, most of the organic fluorophores are hydrophobic compounds that are not soluble in aqueous media. Indeed, when used as carrier in water, polymeric micelles are capable of encapsulating hydrophobic dye in their core, thus enhancing the solubility in water. For example, Cho et al. incorporated an hydrophobic NIR probe, a carbocyanine dye in PEG-*b*-PCL micelles [97]. The results showed that the micelles improved the solubilization of the NIR probe in water. These polymeric micelles with NIR probe seem to be a promising fluorescent imaging agent that will provide a basis for enhanced surgical guidance *via* NIR visualization of tumors.

Inorganic dyes such as quantum dots (QDs) were also encapsulated using degradable polymers. Indeed, in the last decade QDs have attracted considerable interest for their application in optical imaging [98,99]. Although QDs have some benefits compared to organic dyes, such as easy control of the excitation and emission wavelength, high quantum yield in water, or no photobleaching, limitations have been shown as QDs are not water-soluble and not biocompatible [100,101]. Also, encapsulation of QDs using degradable polymers appeared as a promising approach to reduce their potential toxicity, and numerous examples of QDs-loaded NPs are reported in the literature [81,102–112]. The decrease of the toxicity of QDs using encapsulation into NPs has been demonstrated [103], as well as the increase of the solubility of the QDs using micelle NPs [113].

3.3. X-ray and computed tomography imaging modality

As for other imaging modalities, encapsulation of X-ray contrast agents by (co)polyesters in nanocapsules and nanoparticles has been proposed [28,114]. For example the use of PEG_{5k}-*b*-PCL_{11k} copolymers to encapsulate Lipiodol Ultrafluid® and yield nanosized blood pool contrast agents for computed tomography was recently reported [28]. Nanocapsules with an average size of about 150 nm and loaded with 5 wt% iodine (commercially available Fenestra VC® 5.5 wt%) were obtained and injected in mice. The mean half-life of enhanced blood radiopacity was around 4.2 ± 0.5 h. In another approach, tungsten oxide (WO_3) loaded PCL nanoparticles have also been reported and used as blood pool contrast agent *in vivo*. NPs formulations containing a WO_3/PCL weight ratio of 80% injected in mice displayed high X-ray attenuation properties and circulation time up to 3 h [115].

3.4. Ultrasound imaging modality

Ultrasonic imaging is a widely available, non-invasive and cost effective imaging modality, but the weak difference of echogenicity between different tissues often hampers a clear diagnostic. In order to enhance the contrast between specific tissues, ultrasound contrast agents (UCAs) are frequently used [116]. Gas-filled microcapsules are generally used as UCAs due to the superior scattering properties of gas bubbles compared with blood cells. Nowadays, microcapsules are generally made with a shell material and filled in the core with a gas such as perfluorocarbon gas [117,118]. Synthetic polymers, albumin, galactose or lipids can be used as membrane. However, with the development of nanotechnology in polymer chemistry, polymeric microcapsules have recently received great attention for ultrasound imaging due to their better stability than liquid and lipid microcapsules [119–121]. The combination of a biocompatible polymer and fluorinated gas, displaying a low solubility in blood, increased the plasmatic half-life of UCAs [122]. Moreover, it has been proved that the polymeric shell improved the stability of the capsules as compared to the commercially available UCAs [123]. In order to visualize specific tissues via an active targeting, the surface modification of polymeric microcapsules was reported to improve the local accumulation of the UCA [124]. The microcapsules were composed of PLAGA encapsulating a liquid core of perfluorooctyl bromide. Capsules were obtained by a solvent emulsification–evaporation process with functional phospholipids (fluorescent, pegylated and biotinylated). The pegylation did not modify the echographic signal arising from capsules. Recently, a series of polyester-based microcapsules were prepared by Liu et al. [125]. The signal duration of the PLA and PLA-*b*-PEG microcapsules could reach ca. 3 and 3.5 min

continuously. The ultrasound signal intensity and duration of the signals of PLLA microcapsules were considerably stronger and longer than those of commercially available UCAs, showing that the PLLA microcapsules have a great potential for biomedical imaging. For theranostic applications, DOX was encapsulated in the PLA shell of UCA microcapsule [126,127]. In these examples, microcapsules have been used as drug delivery carrier by loading drugs and as contrast agent for ultrasound imaging. Beside pure UCAs, polyester micro and nanocapsules have also been used for dual modality imaging. As mentioned in Section 3.1, the combination of MRI CAs and fluorocarbon gas has been proposed with PLA/SPION and PEG-*b*-PLA/SPION [57–59] or PLGA/Gd-DTPA [67] systems.

4. Functional (co)polyesters as macromolecular contrast agents

Similarly to particulate systems entrapping CAs, macromolecular conjugates, also known as macromolecular contrast agents MCAs, are powerful tools to reach high concentration of contrast agent while overcoming the already mentioned limitations of low molecular weights CAs (rapid clearance, non-specific distribution, toxicity). However, some differences should be noted. First, in opposition to CAs entrapment, the synthesis of MCAs requires chemistry at the molecular level on the polymer backbone, which might raise difficulties in the frame of degradable polymers like the aliphatic polyesters (Scheme 1B). Second, from a regulatory point of view, MCAs might be considered as new compounds and therefore rise concerns with respect to approval. But MCAs offer important advantages over the particulate entrapment approach. The main advantage relies in the control that is offered by this approach, making possible to finely tune the MCAs characteristics to get optimal imaging properties. In addition, covalent bonding of the CA to the polymer backbone excludes any CA leakage. Last, broader applications may be accessible as MCAs can be considered in most cases as thermoplastics that may be used in classical industrial processes, for example as coatings or basic component for polymer medical devices. The following aims at reporting the various approaches that have been proposed for the preparation of aliphatic polyesters based MCAs for imaging or theranostic approaches.

4.1. MRI

4.1.1. MRI polyesters conjugates and functional copolyesters

4.1.1.1. Polycondensates. In a direct synthetic approach, DTPA dianhydride has been used in polycondensation with different kinds of α,ω-diols to form low molecular weights polyesters and oligoesters bearing Gd chelating units along the polymer backbone [128–130]. The resulting polyesters have relaxivities in the range of 5–15 $mM^{-1}\ s^{-1}$. For example, Yan et al. reported on the synthesis of polyesters consisting of DTPA, pentaerythritol and ethylene glycol (Mn = 9.5 kDa, $Đ$ = 1.7). The polymers have a relaxivity $r1$ = 15 $mM^{-1}\ s^{-1}$ and could be further functionalized with pyridoxamine for liver targeting and imaging [131].

4.1.1.2. Dendrimers/stars. Dendrimers are widely considered for diagnostic and theranostic applications. However, an important question reported with dendrimer-based therapeutics to date is their long-term viability and biocompatibility. A number of dendritic contrast agents (DCAs), mainly based on poly(propylenimine) (PPI) and poly(amidoamine) (PAMAM), have been prepared. However, their applications are hindered by their non-degradability which causes serious toxic effects. The sound design of biocompatible dendrimers is therefore a current mater of researches that has been discussed in detail in a recent review by Cheng et al. [8]. Among biocompatible dendrimers, some examples based on PEG or PLL have therefore been proposed. However, these structures are beyond the scope of the present review. For that reason, the following focuses on biocompatible dendrimers based on aliphatic polyesters cores.

Amphiphilic multiarm star block copolymers possessing a fourth-generation hyperbranched polyester (Boltorn™ H40 (BH40)) as the core, a hydrophobic PCL inner layer, and a hydrophilic outer corona of poly(oligo(ethylene glycol) monomethyl ether methacrylate) (POEGMA) covalently labeled with Gd-DOTA and folic acid (FA) for synergistic targeted drug delivery and MR imaging have been proposed. T1 relaxivity for unimolecular micelles was 18.1 $mM^{-1}\ s^{-1}$ compared to 3.1 $mM^{-1}\ s^{-1}$ for that of the small molecule counterpart, alkynyl-DOTA-Gd [132]. In a similar approach, hyperbranched polyester BH40 was derivatized with ethylenediaminetetracetic acid (EDTA) or DTPA groups to yield BH40-EDTA-PEG-FA and BH40-DTPA-PEG-FA bearing 17 chelating groups and 3 PEG chains per dendrimer. Complexation with Gd was almost quantitative in the case of DTPA (95%) compared to EDTA (30%) and relaxivities $r1$ = 12.3 and 7.1 $mM^{-1}\ s^{-1}$ were measured, respectively [133].

Polyester dendrimers using β-cylcodextrin as the core-forming compound was reported by Ye et al. [137]. The one-pot per generation method used was based on the sequential click coupling of cysteamine and 2-[(methacryloyl)oxy]ethylacrylate. Terminal amino groups were then reacted with DTPA–*N*-hydroxysuccinimide (DTPA–NHS) to form dendritic ligand (Fig. 3C). The third generation dendritic contrast agent had a hydrodynamic diameter of 9 nm and relaxivity $r1$ = 11.7 $mM^{-1}\ s^{-1}$. One limitation, however, was the introduction of hydrophobic β-cyclodextrin core into the DCAs that gave a poor solubility in water. In incremental work, to obtain tumor targeting properties, folic acid and PEG_{2k} were therefore grafted onto the dendrimer to further increase blood circulation time and introduce targeting ability [136]. In that case relaxivity $r1$ increased to 17.1 $mM^{-1}\ s^{-1}$ per Gd probably due to the increased solubility and rigidity of the dendrimer. More recently, tris(2-aminoethyl)amine core was also proposed [138].

4.1.1.3. Functional water-soluble (co)polymers. Grogna et al. used α-acetal-PEG-OH to polymerize ε-caprolactone and yield well-defined α-acetal-$PEG_{1.3–4k}$-*b*-$PCL_{1.5–2.6k}$ [139]. Conversion of acetal into aldehyde allowed the grafting of the Gd complex (S-2-(4-aminobenzyl))-DTPA in mild conditions to finally yield the MCA (Gd-DTPA)-PEO-*b*-PCL. Micelles were prepared with hydrodynamic diameter between 20 and 50 nm and relaxivities $r1$ around 10 $mM^{-1}\ s^{-1}$. Based on the same copolymer ($PEG_{2.8k}$-*b*-$PCL_{1.8k}$) multimodal imaging and tumor targeting were also obtained by incorporation of the NIR-dye 1,1-dioctadecyl-3,3,3,3-tetramethyl indotricarbocyanine iodide (DiR) in the PCL core of the micelles and use of FA moieties. Micelles with an average diameter of D$h \approx$ 56 nm and relaxivity $r1$ = 13 $mM^{-1}\ s^{-1}$ were obtained and demonstrated preferential accumulation in tumor tissues on nude mouse bearing xenografted breast tumor [140]. A diblock copolymer with a linear PCL block associated to a brush POEGMA block was also synthesized by combination of ROP and ATRP [134]. POEGMA segments were either associated to Gd-DTPA or folate by CuAAC click chemistry to yield mixed micelles (D$h \approx$ 28 nm) with both imaging ($r1$ = 26 $mM^{-1}\ s^{-1}$) and targeting abilities that were able to deliver PTX (Fig. 3A). DTPA was also conjugated to the hydroxyl PEG chain-end of PEG-*b*-PLA copolymers. Gd was chelated on the DTPA groups exposed at the surface of the formed nanoparticles (D$h \approx$ 265 nm) allowing a relaxivity $r1$ = 18.9 $mM^{-1}\ s^{-1}$ [141].

Macromolecular architectures combining polypeptides and polyesters blocks led to elegant approaches. For example mixed micelles self-assembled from (i) PEG-b-P(L-LA) block copolymers

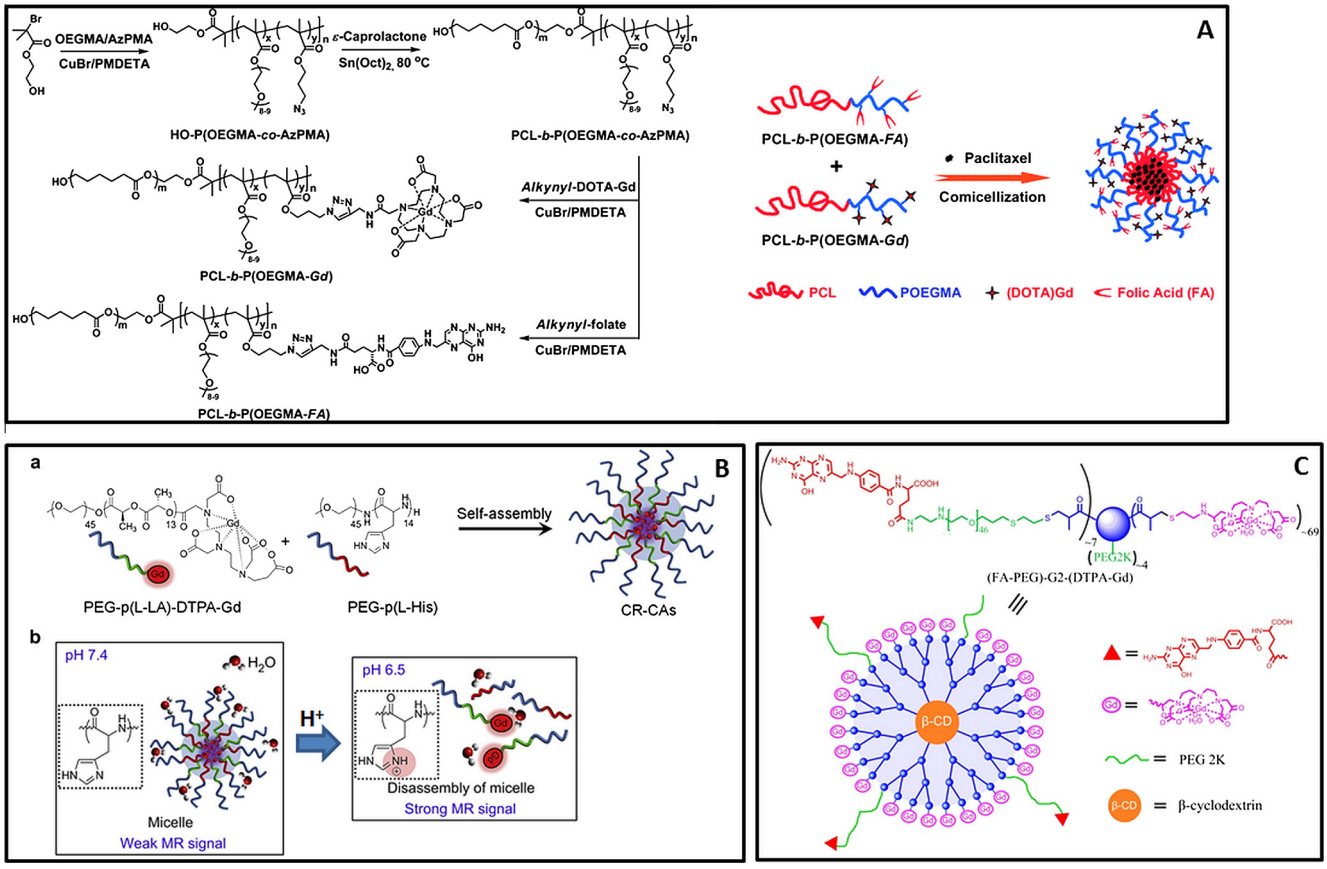

Fig. 3. Examples of (co)polyesters conjugated to Gd-chelates for the formation of nano-objects with MRI capacities. (A) PCL-based copolymers for the preparation of mixed micelles used as theranostic tools (reprinted with permission from Liu et al. [134]); (B) schematic representation of the preparation of pH-responsive theranostic micelles as cancer-recognizable MRI contrast agents (CR-CAs) (a), and of their pH-dependent structural transformation leading to MR signal change (b) (adapted with permission from Kim et al. [135]) and (C) polyester dendrimers gadolinium chelates with b-cylcodextrin core (adapted with permission from Ye et al. [136]).

with PLA chain end functionalized with Gd-DTPA chelate and (ii) poly(ethylene glycol)-b-poly(L-histidine) (PEG_{2k}-*b*-$P(L\text{-}His)_{5k}$) were recently proposed by Kim et al. [135]. The MRI-visible micelles ($r1 = 4.3\ mM^{-1}\ s^{-1}$) were pH-responsive with a spherical shape ($Dh \approx 40$ nm) at physiological pH (pH = 7.4). However, in acidic tumor environment (pH 6.5), they were destabilized and broke apart into positively charged water-soluble polymers. As a result, these micelles exhibited highly effective T1 MR contrast enhancement in the tumor region with detection of small tumors of ~3 mm^3 *in vivo* at 1.5 T within a few minutes (Fig. 3B).

Poly(L-glutamic acid)-*b*-poly(lactide) (PGLA-*b*-PLA) micelles with paramagnetic Gd^{3+} ions chelated to their shell have also been proposed. $PGLA_{7k}$-*b*-PLA_{5k} was synthesized by sequential polymerization reactions: anionic polymerization of L-lactide followed by ring-opening polymerization of benzyl glutamate N-carboxylic anhydride. DTPA was conjugated to about 40% of the side chain carboxylic acid groups of PGLA. Spherical micelles could be obtained with an average diameter of 230 nm at pH 7.4 and T1 relaxivity $r1 = 7.9\ mM^{-1}\ s^{-1}$ compared to $4.3\ mM^{-1}\ s^{-1}$ for Gd-DTPA [142]. A more complex macromolecular architecture was reported by Liu et al. [9]. A triblock copolymer, namely $PLA_{7.5k}$-*b*-PEG_{2k}-*b*-PLL_{2k}, was synthesized by ROP of Lys-NCA from a $PLA_{7.5k}$-*b*-PEG_{2k}-NH_2 macroinitiator. Following deprotection of PLL block, DPTA was reacted with the amine groups of lysine moieties. Finally, multifunctional NPs were prepared by chelation of Gd and conjugation of VEGF antibody on the amino group of PLL exposed on the surface of the NPs ($Dh \approx 85$ nm; $\xi = 21$ mV). The nanoparticles allowed tumor MR imaging over 12 h thanks to a relaxivity $r1 = 18.4\ mM^{-1}\ s^{-1}$, as well as tumor targeting ability as demonstrated *in vivo* with mice bearing subcutaneous H22 cell xenografts tumor model.

4.1.1.4. Hydrophobic MMCAs. It is noteworthy that all the strategies described so far in this review rely on water-soluble amphiphilic copolyesters or nanoparticles. Indeed, water-solubility and/or long term circulation ability are of course prerequisites in the frame of the classical applications of MRI-visible polymers including diagnostic and theranostic tools in oncology, intracellular trafficking and so on. On the other hand, an opposite approach was followed by our group as we focused on the preparation of hydrophobic MRI-visible polyesters to be used as coatings on implantable polymeric medical devices to allow their detection. In a first approach, copolyesters bearing Gd-DTPA derivatives were synthesized by anionic post-polymerization modification of PCL [143]. The main advantage of this synthetic pathway is the possibility to produce large amounts of products at the multigram scale. Following activation by a non-nucleophilic base, a PCL polycarbanionic intermediate was allowed to react with benzylated-DTPA, which was then deprotected prior to Gd chelation. The final PCL-based MCA ($Mw = 20$ kDa, ≈1 mol% Gd-DTPA with respect to CL units) was easily sprayed on surgical meshes and allowed MR stable detection over a 1 year period (Fig. 4). Although interesting for scaling-up, this post-polymerization modification lacks control of parameters that are known to influence the resulting MR signal enhancement like the overall amount of Gd, or its repartition along the polymer chain [144]. To overcome this limitation, a second strategy was proposed based on the synthesis of functional lactones, namely, α-propargyl-caprolactone or 5-amino-δ-valerolactone, to yield

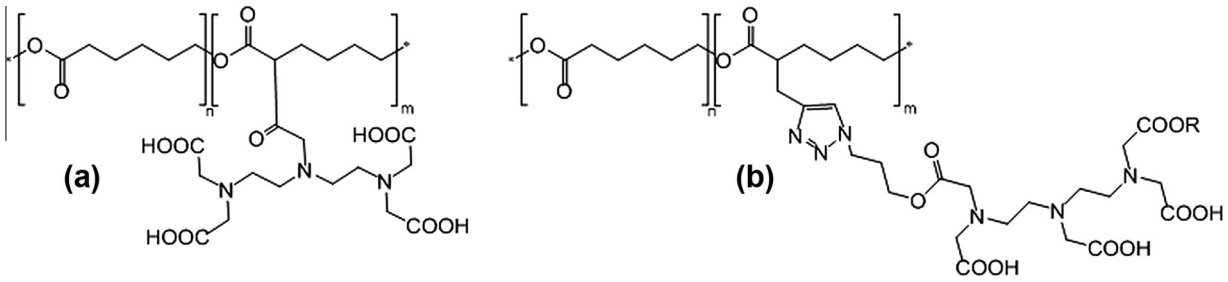

Fig. 4. PCL-based MCAs structures before Gd chelation obtained by (a) anionic post-modification and (b) copolymerization (R = OH or $C_3H_6N_3$) (reprinted with permission from Blanquer et al. [143] and El Habnouni et al. [145]).

well-defined functional PCLs by copolymerization with ε-caprolactone and thus get control over Gd content. For example, poly(α-propargyl-ε-caprolactone-*co*-ε-caprolactone)s containing 2, 5 and 10 mol% (Mw = 20–30 kDa) of propargyl groups were obtained and conjugated with diazido-Gd-DTPA via a Cu^{I}-catalyzed [3 + 2] cycloaddition. MRI-visible PCLs containing 0.8, 2 and 3 mol% of Gd were obtained and showed 70% decrease of T1 relaxation time compared to pristine PCL already with 0.8 mol% of Gd on the polymer while no further decrease above 2 mol% was observed (Fig. 4) [145].

4.1.2. MRI labeling of polyester surfaces

As shown in the first paragraph, NPs for medical imaging attract tremendous attention, in particular as they offer viable platforms for targeted theranostic tools. With aim to benefit from these advantages while improving MR sensitivity of SPION embedding NP and/or avoiding the rapid diffusion of hydrophilic low-molecular weight Gd-chelates out of NPs some authors reported on surface modification of PLA or PLGA nanoparticles to yield particulate CAs with mono- or multimodal imaging capabilities.

For example Cheng et al. developed PLGA NPs embedding FITC whose surface was modified by pegylated quantum dots for dual optical imaging or by amino SPION for MRI imaging [95]. PEG-NH2 modified quantum dots (PEG-NH2-QD) or amine functional SPION were conjugated at surface of stabilizer-free PLGA NPs on the available chain-end carboxylic groups. The $r2$ relaxivity of SPIONs–PLGA NPs with sizes of 70 and 190 nm was $r2$ = 294 and 817 $mM^{-1}\ s^{-1}$, respectively, compared to 85 $mM^{-1}\ s^{-1}$ for the bare SPIONs.

PLA NPs loaded with DOX (7 wt%) were also covalently functionalized by Mn-porphyrin (Mn-P) used as T1 agent [146]. Again, amino-functional Mn-P was conjugated to the NPs surface by using EDC/NHS activation leading to a manganese content of 1.3 wt%. The mean diameter of MnP–DOX NPs was 100 nm whereas their zeta potential was strongly negative with $\xi = -37$ mV. MRI visibility was confirmed *in vitro* with a relaxivity $r1$ found equal to 27.8 $mM^{-1}\ s^{-1}$ for the NPs compared to 6.7 $mM^{-1}\ s^{-1}$ for free Mn–PNH_2. In another approach, Ratzinger et al. immobilized DTPA and DOTA ligands on branched poly(ethylenimine) (PEI), at the surface of PLGA NP via a double NHS activation prior to Gd chelation [147]. Gd-loaded NP had a mean diameter of nearly 200 nm and Gd loadings reached 235 $\mu g\ mg^{-1}$ of PLGA for Gd-DTPA-PEI-NP or 150 $\mu g\ mg^{-1}$ of PLGA for Gd-DOTA-PEI-NP. Relaxivity $r1$ was found in the range 12–16 $mM^{-1}\ s^{-1}$ with respect to Gd concentration. Although promising, the main reported drawback of this approach was the required successive dialyses to eliminate the noncomplexed Gd, which resulted in partial degradation of the PLGA particles. Finally, an original approach based on the microwave driven growth of iron-enriched carbon nanotubes (CNT-Fe) on the surface of PTX loaded PLGA microparticles was recently reported to yield MRI and drug delivery tools [148]. Three steps were needed to grow (CNT-Fe) on the particles, namely (i) the *in situ* deposition of a layer of polypyrrole, (ii) the mixing of the resultant coated particles with ferrocene and (iii) microwave irradiation leading to a rapid rise of temperature and therefore the decomposition of ferrocene to iron nanoparticles and cyclopentadienyl groups, where iron nanoparticles serve as the catalyst and the carbon atoms pyrolyzed from cyclopentadienyl ligands serve as the carbon source. The resulting nanoparticles had an average size of 50 nm and showed a T2 effect.

4.2. Optical imaging

4.2.1. Polyesters labeled with fluorophores

As mentioned previously, one of the main drawbacks of the fluorophore physical encapsulation is that the dye can leak out of the nanoparticles with time. To circumvent this shortcoming, the fluorophore can be linked to the NPs by covalent ligation and the covalent labeling can be achieved either during the synthesis of the polymers or by surface modification of the polymeric NP (Scheme 1B). However, to the best of our knowledge examples dealing with the second approach based on the fluorophore-decorated NP are rare. Indeed, use of labeled polymer backbones for encapsulation of fluorescent probes into the NPs is generally preferred in order to improve the biocompatibility and the stability of the fluorescents probes. With the recent improvements in macromolecular engineering, a large variety of fluorescent polymer conjugates has been reported in the literature. These fluorescent polymers are then able to self-assemble in various nanostructures including nanospheres, micelles, and vesicles.

Fluorescent polyesters can be synthesized by ring opening polymerization of lactones such as lactide, glycolide or ε-caprolactone using a fluorescent initiator bearing a hydroxyl group able to initiate ROP. For instance, tetra and hexahydroxy functionalized perylene chromophores have been used as initiator for the ROP of lactones (Fig. 5A) [153]. More recently, difluoroborondibenzoyl methane-PLA was synthesized by ROP of lactide using a hydroxyl-functionalized difluoroborondibenzoylmethane initiator (Fig. 5B) [149,150]. Then, well-defined nanoparticles were prepared by nanoprecipitation. Strong fluorescence and absence of cytotoxicity for the NPs were observed. Interestingly, the fluorescence was tunable with the molar mass of the functional PLA. This system can be considered as a dual-emissive NP as both emissions in fluorescence and phosphorescence were observed (Fig. 5E). Other fluorescent polyesters using different classes of fluorescent initiators were reported in the recent year [151,152].

Another approach is based on the post-modification of preformed polyester. Reul et al. synthesized NIR fluorescent polyester by chemical modification of PLGA (Fig. 5C) [154].

The carboxyl moiety of PLGA was activated by reaction with NHS before amidification with the amine moiety of the NIR probe to yield NIR-PLGA conjugate. Incorporating 1% of this conjugate

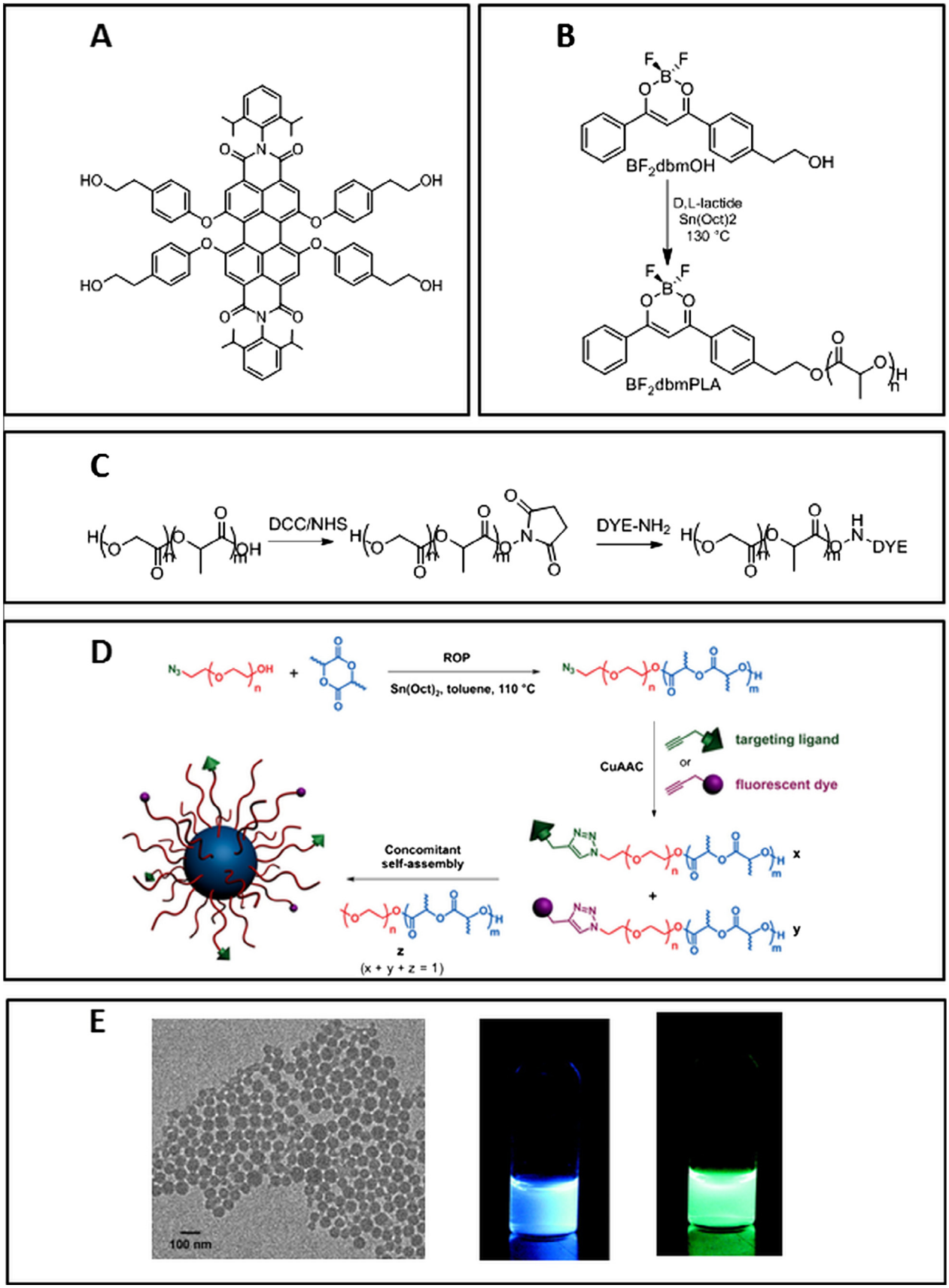

Fig. 5. Examples of structures with optical imaging capacities. (A) Fluorescent tetrahydroxyperylene used as initiator for the ROP of lactide (adapted with permission from Klok et al. [153]), (B) functional poly(lactide) (BF_2dbmPLA) prepared by ROP of lactide using a functional initiator (adapted with permission from Zhang et al. [149]), (C) synthesis of near-infrared labeled PLAGA for *in vivo* imaging (adapted with permission from Reul et al. [154]), (D) synthesis of tunable targeted and fluorescent PEGylated poly(lactide) nanoparticles by a combination of ROP, CuAAC, and concomitant self-assembly into nanoparticles in aqueous solution (reprinted with permission from Mackiewicz et al. [155]) and (E) TEM image, fluorescence and phosphorescence of BF2dbmPLA NPs (reprinted with permission from Pfister et al. [150]).

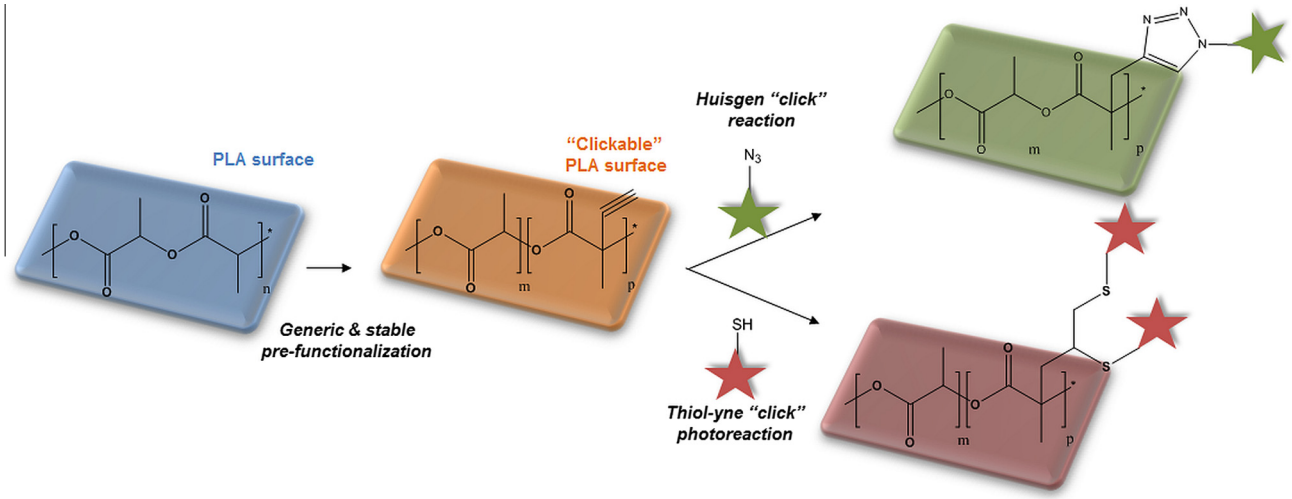

Scheme 2. Fluorescent labeling of PLA surfaces via click chemistries. (Adapted with permission from El Habnouni et al. [162] and Sardo et al. [163].)

into PLGA nanoparticles leads to stable NPs showing strong fluorescence and biocompatibility that were suitable for *in vitro* and *in vivo* imaging.

With the emergence of efficient ligation such as "click chemistry" and the renewal of interest of forgotten chemical reaction, other fluorescent polyesters were reported using different classes of fluorescent tags [155–159]. Pendent functionalization of aliphatic polyesters can be achieved by polymerization of functional lactone and post-polymerization modifications using for example click chemistry [157]. In another example, multifunctional PEG-*b*-PLA nanoparticles for cancer cell targeting and imaging have been designed by a combination of ring-opening polymerization and "click" chemistry (Fig. 5D) [155]. A large library of nanoparticles such as ligand-decorated nanoparticles (with biotin, folic acid or anisamide) and fluorescent nanoparticles (UV–vis or near-infrared dyes) was prepared. *In vitro* cancer cell targeting was successfully demonstrated on different cancer cell lines notably through confocal microscopy.

4.2.2. Fluorescent labeling of polyester surfaces

In the past few decades, surface engineering approach has been extensively explored in order to bring new functionalities to polymeric biomaterials. Among other aspects, monitoring the fate of polymeric biomaterials using non-invasive molecular imaging is fundamental in biomedical applications. To achieve this, the functionalization of surface via covalent coupling is one of the most important strategies. Nevertheless, most of the classical coupling reactions available for surface chemistry are limited in such conditions due to incomplete conversion, non-specificity, and harsh reaction conditions. In this context "click chemistry", especially the copper-catalyzed azide-alkyne cycloaddition, has proven to be a powerful tool to functionalize surfaces due to the mild reaction conditions, high conversions, selectivity and reproducibility [160]. As mentioned previously, very few examples of fluorescent surface-labeled biodegradable nanoparticles have been reported in the literature [161]. Recently, our group reported the fluorescent labeling of PLA surfaces by chemical modifications (Scheme 2). After the synthesis of alkyne-functionalized PLA surface by anionic modification, fluorescent probes bearing azido group or thiol groups were grafted to the PLA surface by Huisgen "click" reaction [162] or photoradical thiol-yne addition [163]. It is noteworthy that only surface modification occurred without bulk modification or degradation of the material.

4.3. X-ray and computed tomography imaging modality

4.3.1. Polyesters and metallic radio-opacifiers

Polymeric biomaterials featuring radio-opacity continue to attract considerable scientific attention since it is highly desirable to visualize medical devices such as cardiovascular implants, prostheses, orthopedic implants *via* routine X-rays computed tomography. However polymeric biomaterials are transparent to X-rays and when a polymeric biomaterial has to be implanted in the human body, it is often made radio-opaque by addition of an X-ray absorbing additive such as metal powders, metal salts based on tantalum, barium, bismuth and gold [164–167]. For example Lamsa et al. reported on radiopaque stents composed of PLA96 with 25 wt% of $BaSO_4$ that were used as radiopaque bioabsorbable biliary stents [168,169]. To avoid leaching of potentially metallic compounds, organic–inorganic hybrid was prepared via the sol–gel process starting from a dihydroxy-terminated polyester poly(1,4-butyleneglutarate) (PBG) and a titanium alkoxide (TIPT) as precursors [170]. It was demonstrated that a transesterification reaction of the polymer chain occurring *in situ* led to organotitanium esters connecting organic and inorganic domains. Interestingly, even with up to 50 wt% of TIPT, the final hybrid material was still transparent, while demonstrating radio-opacity. In an incremental work, this approach was enlarged to PLA and PCL [171].

4.3.2. Polyesters and organic radio-opacifiers

Another alternative to circumvent the potential toxicity of metallic additives [172] is the chemical conjugation of organic radio-opacifiers containing heavy atoms as bromine or iodine. In most cases iodinated opacifiers are covalently linked to the polymers or, in a preferred approach, iodinated monomers are copolymerized to yield radiopaque copolymers. This methodology has been applied to various polymeric materials including cellulose [173,174], poly(meth)acrylates [22,175–186], polyurethanes [25], polyphosphazenes [187] or polycarbonates [188]. Regarding polyesters, like for inorganic radiopacifiers, the most common approach relies on the use of polyester/radio-opacifier blends with problems of leaching of the later. To avoid leaching, Wang et al. reported recently on biocompatible and PLA-miscible iodinated contrast agent, namely (S)-2-hydroxy-3-(4-iodobenzyloxy) propanoic acid that has a plasticizing effect due to structural compatibility with PLA [189]. The blend obtained with 10 wt% contrast agent yielded

about 25% attenuation compared to aluminum. However, no covalent bond is found between the PLA backbone and the organic opacifier. Indeed, very few studies report on aliphatic polyesters conjugates for X-ray modalities. To the best of our knowledge, the first radio-opaque polyester bearing iodine was described by Nottelet et al. [190]. Poly(ε-caprolactone-*co*-α-iodo-ε-caprolactone) was synthesized by introducing iodine in the α position of the carbonyl group of PCL thanks to the anionic modification presented in Section 4.1.1 (Fig. 6A). Copolyesters containing from 10% to 25% of iodized units were thus obtained. In another strategy iodinated PCLs were prepared by copolymerization of α-iodo-ε-caprolactone with ε-caprolactone (Fig. 6B) [191,192]. The X-ray opacity was assessed, and appeared high enough to be of interest for biomedical applications although stability of carbon-iodine bond could be improved.

More recently, radio-opaque biodegradable polyesters have been prepared by ring-opening polymerization of lactide and ε-caprolactone using an iodinated initiator, namely 2,2-bis(hydroxymethyl)propane-1,3-diyl bis(2,3,5-triiodobenzoate) (Fig. 6C) [193]. The resulting polyesters (Mw = 11–66 kDa) exhibited a radio-opacity of 60–124% relative to an aluminum sample of the same thickness and could be electrospun into nanofibers.

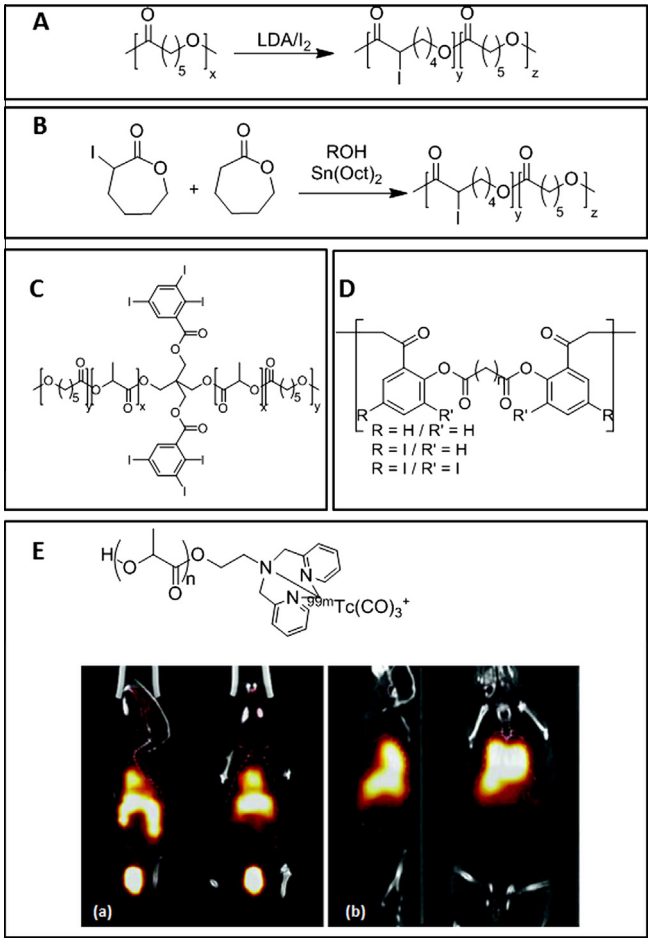

Fig. 6. (A) Iodinated-PCL prepared by anionic post-modification of native PCL (adapted with permission from Nottelet et al. [190]); (B) iodinated-PCL prepared by copolymerization of α-iodo-CL and CL (adapted with permission from El Habnouni et al. [191]); (C) structure of iodinated star polyesters (adapted with permission from Rode et al. [193]); (D) structure of iodinated poly(anhydride-ester)s (adapted with permission from Carbone et al. [194]) and (E) structure of ^{99m}Tc radiolabeled poly(lactide) and microSPECT/CT images of (a) $[^{99m}Tc(H_2O)_3(CO)_3]^+$ and (b) ^{99m}Tc radiolabeled PLA microspheres 6 h after tail vein injection (sagittal view left, and coronal view right) (adapted with permission from Saatchi et al. [195]).

Similarly, biodegradable radiopaque iodinated poly(ester-urethane) based on PCL_{2k} and iodinated bisphenol containing up to 30 wt% iodine [196], or salicylate-based poly(anhydride-ester) [194], have been reported (Fig. 6D). It should be noted that, whereas attenuation similar or even higher than aluminum and good cytocompatibility were shown with the poly(ester-urethane)s, cytotoxicity was observed toward L929 mouse fibroblasts with the iodinated salicylate-based poly(anhydride-ester)s. The recent development of these series of radiopaque and biodegradable polyesters confirms the renewed interest in X-ray macromolecular contrast agents. In this frame the presented polyesters appear to be promising candidates for medical imaging where radio-opacity of implants is an important parameter.

4.4. Radiolabeled polyester for radionuclide imaging

Few examples of radiolabeled polyesters are reported in the literature. One of the first examples was poly(lactide) (PLA) labeled with radioactive tritium, obtained by chemical modification of preformed PLA [197]. More recently, PLA microspheres tailored with a tridentate chelating group were radiolabeled with ^{99m}Tc for SPECT imaging (Fig. 6E) [195]. Those microspheres exhibit excellent radiolabeling efficiency and radiochemical stability. The radiolabeling of aliphatic polyester-based dendrimer with ^{99m}Technetium was reported by Parrot et al. [198]. The distribution of the radiolabeled dendrimers was evaluated in healthy adult Copenhagen rats using dynamic small-animal SPECT tomography. The labeled dendrimers were cleanly and rapidly eliminated from the bloodstream via the kidneys. The quantitative biodistribution results were in excellent agreement with the data obtained from the dynamic SPECT images. Other examples based on the radiolabeling of polyesters for SPECT imaging are reported in the literature such as ^{111}In-labeled block PCL micelles [199] or ^{123}I-labeled copolyesters [200].

Concerning PET imaging, ^{64}Cu-labeled brush-shaped amphiphilic block copolymers based on PLA and PEG were prepared [201,202]. After self-assembling and encapsulation of DOX, multifunctional theranostic unimolecular micelles were formed with promising applications in cancer theranostics. Another example is based on the ^{18}F-labeled PLAGA nanoparticles, NPs were radiolabeled with biotinylated F-18 prosthetic groups [203]. The radiolabeled NPs were delivered to the brain by convection-enhanced delivery and visualized by PET imaging thus providing information on the fate of the NPs into the brain.

5. Applications

5.1. Cell imaging and intracellular trafficking

Non-invasive cell tracking is an emerging approach for imaging cells in their native environment. By labeling cells with imaging particles, cells location is indirectly reported by detection of the particles. For example non-invasive imaging of the trafficking patterns of phenotypically defined populations of immune cells is used to develop next-generation therapeutics for the treatment of autoimmune disease and cancer [204]. Tissue uptake of PLGA NPs can also provide information for more classical therapeutic approaches such as drug delivery, gene transfer, as well as optimal routes of delivery and therapeutic doses for individuals (Fig. 7A). For example quantum dots conjugated PLGA NPs bearing nuclear localization signal (NLS) peptides (NLS-QD-PLGA NPs) were used to test the ability of NPs to enter the nucleus of cells in the frame of gene therapy or anticancer drug delivery studies [95]. More recently, medical imaging-based cell tracking has also graduated to *in vivo* clinical investigations. For example *in vivo* MRI experiments were performed in rats with PLGA micro- and nanoparticles

embedding SPIONs to separately test cell transplantation and cell migration paradigms [205]. It was reported that MRI detected as few as 10 magnetically labeled cells, transplanted into the brains of rats and the particles enabled the *in vivo* monitoring of endogenous neural progenitor cell migration in rat brains over 2 weeks.

5.2. Early diagnosis (thrombus, cancer) and imaging assisted surgery

Diagnosis has been the keystone of medical imaging development and it is therefore no surprise if most applications for polyesters offering imaging modalities are found in this field. All kinds of diagnosis are covered including the characterization of tumor microvessels thanks to MCAs [206], or the use of SPION-based systems as markers of inflammatory and degenerative disorders thanks to their uptake by the monocyte-macrophage system [16]. Accurate imaging of atherosclerosis for timely treatment of the disease by MRI was proposed based on the use Gd-DTPA PLGA microparticles [61]. In a similar way, an important application is the early thrombus detection and thrombolysis. MR molecular imaging has been proposed for the early detection of thrombi and the dynamic monitoring of the thrombolytic efficiency. Nanocapsules composed of a SPION-loaded PLGA shell that embedded a core of recombinant tissue plasminogen activator (rtPA) as thrombolytic drug was recently reported by Zhou et al. [207]. The surface of the nanocapsules was modified with a RGD-chitosan conjugate to ensure targeting properties toward thrombus as RGD is a receptor antagonist of platelet membrane glycoprotein GP IIb/IIIa that has a tendency to bind activated platelets at the thrombus site and to adhere to the surface of the thrombus.

Another main application is of course the detection of tumor tissues where all imaging modalities are represented. For example, accurate diagnosis in early stage of hepatocellular carcinoma thanks to PEG-*b*-PLA Gd-DTPA micelles [63] or targeted multifunctional NPs bearing Gd-DTPA and VEGF antibody [9] was proposed. FA-PEG_{4k}-*b*-PCL_{1-7k} micelles developed by Cheng et al. were evaluated *in vivo* for tumor targeting and showed prolonged circulation and slower liver accumulation. In addition, enhanced accumulation within xenografted Bel7402 tumor was confirmed with MRI signal visible from 0.5 h to 24 h after tail vein injection in nude mice (Fig. 7Ba) [85]. FA-targeted polyesters-Gd dendrimers were used to enhance *in vivo* MRI visibility of tumor [136]. Nude mice inoculated with human KB tumors were intravenously injected with targeted dendrimer or Magnevist (same dose of 0.1 mmol Gd/kg). The tumors contrasted by the dendrimer were much brighter than those contrasted by Magnevist with about twice higher contrast-to-noise ratio. In addition significantly longer retention in tumor was observed allowing for marked identification of tumor from normal tissues and clear demarcation of tumor boundary (Fig. 7Bb). In another MRI-based example specific targeting for early diagnosis of breast cancer was achieved through the use of dual ligand targeted magnetic micelles composed of PEG-*b*-PCL embedding SPION and decorated with both cRGD, binding to the $\alpha_v\beta_3$ integrin of endothelial cells of tumor neovasculature, and single chain HER-2 antibody fragment (scFv-ErbB), for human epidermal growth factor repector-2 overexpressed in breast tumor cells [208].

A whole animal NIR imaging approach was used to investigate the tumor targeting and the *in vivo* distribution in nude mice of the FA-ICG-PLGA-lipid NPs described in Section 3.2 [87]. It was demonstrated that free ICG and ICG-PLGA-lipid NPs were mostly located in the intestine 8 h post-injection and did not provide detectable signal 24 h post-injection. In contrast, the targeted FA-ICG-PLGA-lipid NPs were mostly located around the tumor at 8 h, and retained significant fluorescence signal in the tumor at 24 h Fig. 7C. Then, FA-ICG-PLGA-lipid NPs clearly displayed the tumor against surrounding tissues, which was good evidence of the high efficiency of tumor targeting of these NPs.

Long-circulating positron-emitting magnetic nanoconstructs (PEM) were also proposed by Aryal et al. to image solid tumors for combined PET/MRI [79]. PEMs with SPION-loaded PLGA core and a phospholipidic shell composed of PEG or DOTA/Cu-64 coupled lipids were prepared. PEMs have diameter of about 140 nm and relaxivity $r2 = 265.0\ mM^{-1}\ s^{-1}$. *In vivo*, using a murine xenograft model bearing human breast cancer cell line, intravenously administered PEMs progressively accumulated in tumors reaching a maximum of 3.5% injected dose/g tumor at 20 h post-injection thus allowing detailed interrogation of disease status over multiple scales (Fig. 7D).

Finally, imaging-assisted surgery is also proposed. For example, SPION-embedding $PLGA_{20k}$ microcapsules ($Dh \approx 900$ nm) demonstrated their potential as dual contrast agents for ultrasonography and magnetic resonance imaging *in vivo* with enhancement of high intensity focused ultrasound (HIFU) ablation of breast cancer in rabbits Fig. 7E [209].

5.3. Theranostic applications

Most major diseases offer potential applications for the theranostic tools described in this review. In fact depending on their nature, these tools can offer targeting modalities in addition to imaging and drug delivery possibilities. In the case of magnetic particles, magnetic targeting is of course one interesting approach. For example SPION-loaded PLGA NPs were targeted to the inner ear through the cochlear round window membrane (RWM) that may provide an entry for delivery of bioactive molecules for protection against sensorineural hearing loss [211]. In another example, PLGA microparticles embedding FeCO nanoparticles were designed for MRI steering and chemoembolization of liver tumors [212]. But SPION-loaded carriers are also used without steering. For example, they were used for the targeted delivery of nanovaccine particles (NPs) to dendritic cells (DC) *in vivo* as it is a promising strategy to enhance immune responses. Cruz et al. reported on NPs to allow multimodal imaging of nanocarrier DC interactions. These pegylated PLGA NPs were encapsulating fluorescent labeled SPION and targeted delivery was facilitated by coating the NPs with antibodies recognizing the DC-specific receptor DC-SIGN (Fig. 7A) [210]. In oncology, PEG-*b*-PCL nanomicelles modified with anti-EGFR monoclonal antibody and loaded with DOX and SPION have been proposed as a MRI-visible and targeted drug delivery agent for targeting EGFR-overexpressing tumor cells [213]. PTX (1.8 wt%)/SPION (10.4 wt%) loaded PLGA-based nanoparticles with a size of 240 nm have also demonstrated efficacy as both T2 contrast agent ($r2 \approx 130\ mM^{-1}\ s^{-1}$) and anticancer drug delivery system. PTX/SPION-loaded NPs (PTX 5 mg/kg) induced *in vivo* a regrowth delay in CT26-tumor-bearing mice with higher survival rates than the untreated group (PBS) as shown with median survival rate of 15 days, compared to 9 days [214]. PLGA microparticles (≈1 μm) loaded with the multi-kinase inhibitor sorafenib 18.6% (w/w) and 0.54% (w/w) ferrofluid were also used for local transcatheter delivery of sorafenib to liver tumors and MRI intra-hepatic biodistribution [80].

For gene therapy, PEG-*b*-PLA nanoparticles loaded with SPION and coated with a multilayer of chitosan/polyethyleneimine/plasmid (ratios 5:5:1) were used as theranostic tools for gene delivery [215]. The complex CP–micelles ($Dh \approx 110$–130 nm) have a relaxivity $r2 = 110\ mM^{-1}\ s^{-1}$ and were able to deliver plasmid *in vivo* as confirmed with red-fluorescent protein (Tomato) expression in the liver and prostate observed from day 1 up to day 7 after injection in male mice.

Although less developed than their SPION counterparts, Gd-based theranostic tools are also found. For example, sustained release of angiogenic factors VEGF to treat ischemia was achieved

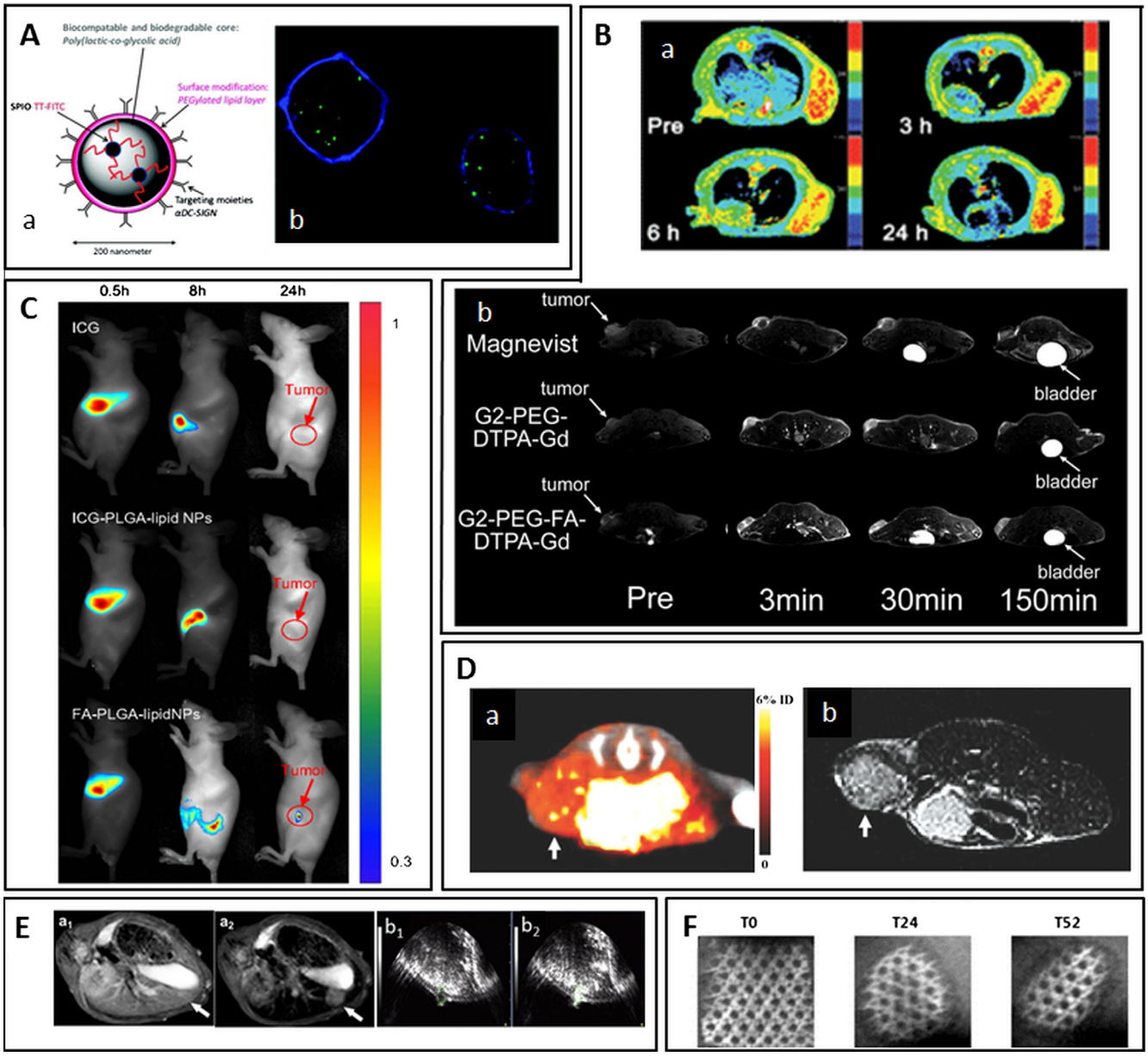

Fig. 7. Examples of applications of polyester-based imaging systems. (A) PLGA NPs with dual-imaging modality for intracellular delivery of vaccines in dendritic cells (DCs): (a) schematic illustration of targeted nanovaccine carrier and (b) NPs uptake by DCs for 1 h (confocal analysis NP in green; cell membrane in blue) (adapted with permission from Cruz et al. [210]); (B) tumor detection and early diagnosis by MRI using targeted NPs: (a) MRI T2 maps acquired before and after tail vein administration of FA–$PEG_{4.3k}$-PCL_{1k}-SPION micelles into mice bearing a Bel 7402 tumor (about 0.5 cm in diameter) at a dose of 10 mg Fe/kg body weight (adapted with permission from Cheng et al. [85]) and (b) 2D axial images of tumors in mice injected with Magnevist, polyesters-Gd dendrimers or folate-targeted polyesters-Gd dendrimers at 0.1 mmol/kg (adapted with permission from Ye et al. [136]); (C) tumor detection and early diagnosis by NIR-imaging using targeted NPs: Free indocyanine green (ICG), ICG-PLGA-lipid NPs and FA-ICG-PLGA-lipid NPs *in vivo* images taken at 0.5, 8, 24 h time point. Fluorescence signal was localized in tumor 8 h and 24 h after administration FA-ICG-PLGA-lipid NPs (reprinted with permission from Zheng et al. [87]); (D) multiscale detection of tumors by peritumoral accumulation of positron-emitting magnetic nanoconstructs (PEMs) (a) co-registered PET-CT image and (b) MR image performed separately 20 h after p.i. of PEMs into a tumor-bearing mouse (adapted with permission from Aryal et al. [79]); (E) imaging-assisted surgery using dual (US + MRI) imaging Fe_3O_4/PLGA microcapsules: *in vivo* MRI of rabbits bearing breast tumor before (a1) and after 5 min (a2) injection of microcapsules (arrows indicate the tumor) and sonographys showing echoes of the targeted tissue in breast tumor before (b1) and after (b2) high intensity focused ultrasound (HIFU) ablation using Fe_3O_4/PLGA microcapsules (adapted with permission from Sun et al. [209]) and (F) follow-up of implantable medical devices: one year *in vitro* follow up of MR visibility of a PCL-based macromolecular contrast agents coated surgical mesh (Adapted with permission from Blanquer et al. [143]). (For interpretation of the references to color in this figure legend, the reader is referred to the web version of this article.)

thanks to the use of Gd-DPTA loaded PLGA NPs [60]. Multi-block copolymer PEG-*b*-P(L-LA)-b-PLL/Gd-DTPA associated to biotin-conjugated PEG-*b*-P(L-His) were used for the preparation of pH-responsive micelles ($Dh \approx 180$ nm, $r1 = 17.3\ mM^{-1}\ s^{-1}$). Anti-hepatocellular carcinoma drug sorafenib was encapsulated inside the micelles (2.4 wt%) whereas biotinylated vascular endothelial growth factor receptor (VEGFR) antibodies were linked to the surface biotin groups through the avidin linker. The pH-sensitive sorafenib release was observed at different pH values with 47.8% at pH 7.4 and 99.3% at pH 5.0, respectively. *In vivo* studies showed high antitumor effect in H22 tumor (VEGFR overexpressed cell line) bearing mice [216].

Of course, it is to note that although many examples of theranostic tools rely on MRI for historical reasons, other imaging modalities are also used with recent examples using optical imaging [127,217] or ultrasound [155].

5.4. Medical imaging of implants

One important application of polymeric biomaterials is their use for medical devices, especially prostheses. Such materials can be used for permanent or temporary applications, but are transparent to X-rays and are invisible using MRI. This inability to visualize implanted material restricts any evaluation of tissue integration and post-operative fixation, and any determination of the fat in the body [218]. Surface modification or coatings are therefore required to overcome this limitation. For this purpose our group developed recently Gd-DTPA-PCL MCAs to be used as MRI-visible coatings. PCL with DTPA-functionalized units were obtained by anionic post-modification or copolymerization and led after Gd complexation to MCAs containing from 0.8 mol% to 3 mol% of Gd with respect to CL units [143,145]. Low amounts of Gd were necessary for the long-term visualization of prosthetic materials as demonstrated on surgical meshes that were made MRI-visible with a dose 1/25,000 compared to the recommended 0.1 mmole/kg for Gd-DTPA bolus injection (Fig. 7F). In addition, beside coatings applications, it was demonstrated that these hydrophobic MRI-visible copolyesters could be used to prepare NPs that may be used for further theranostic tool development [219].

6. Conclusion

Thanks to their biocompatibility, degradability and their long track record in the biomedical field, aliphatic polyesters offer unique opportunities to design systems able to meet medical imaging modalities requirements. The possibility to work with well-known systems, including classical nanoparticles or micelles, or with novel chemical structures thanks to polyester chemistry represent exciting approaches to develop improved and efficient platforms for diagnostic and theranostic applications. For these reasons, and although innovative systems may have to face in the near future the reality of regulatory approval, strategies combining polyesters and imaging surely open the way to better patients and disease management.

References

[1] O. Guillaume, S. Blanquer, V. Letouzey, C. Paniagua, L. Lemaire, F. Franconi, J.P. Lavigne, O. Lefranc, P. Gravagna, R. de Tayrac, J. Coudane, X. Garric, Conception of an anti-infectious and MRI visible mesh used for pelvic organs prolapse and abdominal hernias surgery, Irbm 33 (2012) 78–85.

[2] K.J. Thurecht, Polymers as probes for multimodal imaging with MRI, Macromol. Chem. Phys. 213 (2012) 2567–2572.

[3] S.M. Janib, A.S. Moses, J.A. MacKay, Imaging and drug delivery using theranostic nanoparticles, Adv. Drug Deliver. Rev. 62 (2010) 1052–1063.

[4] V.P. Torchilin, PEG-based micelles as carriers of contrast agents for different imaging modalities, Adv. Drug Deliver. Rev. 54 (2002) 235–252.

[5] A.J.L. Villaraza, A. Bumb, M.W. Brechbiel, Macromolecules, dendrimers, and nanomaterials in magnetic resonance imaging: the interplay between size, function, and pharmacokinetics, Chem. Rev. 110 (2010) 2921–2959.

[6] R. Srikar, A. Upendran, R. Kannan, Polymeric nanoparticles for molecular imaging, WIREs Nanomed. Nanobiotech. 6 (2014) 245–267.

[7] V.V. Mody, M.I. Nounou, M. Bikram, Novel nanomedicine-based MRI contrast agents for gynecological malignancies, Adv. Drug Deliver. Rev. 61 (2009) 795–807.

[8] Y. Cheng, L. Zhao, Y. Li, T. Xu, Design of biocompatible dendrimers for cancer diagnosis and therapy: current status and future perspectives, Chem. Soc. Rev. 40 (2011) 2673–2703.

[9] Y. Liu, Z. Chen, C. Liu, D. Yu, Z. Lu, N. Zhang, Gadolinium-loaded polymeric nanoparticles modified with Anti-VEGF as multifunctional MRI contrast agents for the diagnosis of liver cancer, Biomaterials 32 (2011) 5167–5176.

[10] K.J. Cho, X. Wang, S.M. Nie, Z. Chen, D.M. Shin, Therapeutic nanoparticles for drug delivery in cancer, Clin. Cancer Res. 14 (2008) 1310–1316.

[11] M. Vert, Polymeric biomaterials: strategies of the past vs. strategies of the future, Prog. Polym. Sci. 32 (2007) 755–761.

[12] M. Vert, Degradable and bioresorbable polymers in surgery and in pharmacology: beliefs and facts, J. Mater. Sci – Mater. Med. 20 (2009) 437–446.

[13] B. Nottelet, C. Di Tommaso, K. Mondon, R. Gurny, M. Moller, Fully biodegradable polymeric micelles based on hydrophobic- and hydrophilic-functionalized poly(lactide) block copolymers, J. Polym. Sci. Polym. Chem. 48 (2010) 3244–3254.

[14] M.A. Woodruff, D.W. Hutmacher, The return of a forgotten polymer – polycaprolactone in the 21st century, Prog. Polym. Sci. 35 (2010) 1217–1256.

[15] R. Mathurdevre, Biomedical implications of the relaxation behavior of water related to NMR imaging, Brit. J. Radiol. 57 (1984) 955–976.

[16] C. Burtea, S. Laurent, L. Vander Elst, R. Muller, Contrast agents: magnetic resonance, in: Molecular Imaging I Handbook of Experimental Pharmacology, Springer-Verlag, Berlin, Heidelberg, 2008, pp. 135–165.

[17] S. Laurent, C. Henoumont, L. Vander Elst, R.N. Muller, Synthesis and physicochemical characterisation of Gd-DTPA derivatives as contrast agents for MRI, Eur. J. Inorg. Chem. (2012) 1889–1915.

[18] S. Laurent, D. Forge, M. Port, A. Roch, C. Robic, L.V. Elst, R.N. Muller, Magnetic iron oxide nanoparticles: synthesis, stabilization, vectorization, physicochemical characterizations, and biological applications, Chem. Rev. 108 (2008) 2064–2110.

[19] S. Aime, D.D. Castelli, S.G. Crich, E. Gianolio, E. Terreno, Pushing the sensitivity envelope of lanthanide-based magnetic resonance imaging (MRI) contrast agents for molecular imaging applications, Acc. Chem. Res. 42 (2009) 822–831.

[20] J.V. Frangioni, In vivo near-infrared fluorescence imaging, Curr. Opin. Chem. Biol. 7 (2003) 626–634.

[21] B.A. Smith, S.T. Gammon, S. Xiao, W. Wang, S. Chapman, R. McDermott, M.A. Suckow, J.R. Johnson, D. Piwnica-Worms, G.W. Gokel, B.D. Smith, W.M. Leevy, In vivo optical imaging of acute cell death using a near-infrared fluorescent zinc–dipicolylamine probe, Mol. Pharm. 8 (2011) 583–590.

[22] Z.Y. Wang, T. Chang, L. Hunter, A.M. Gregory, M. Tanudji, S. Jones, M.H. Stenzel, Radio-opaque micelles for X-ray imaging, Aust. J. Chem. 67 (2014) 78–84.

[23] N. Anton, T.F. Vandamme, Nanotechnology for computed tomography: a real potential recently disclosed, Pharm. Res. 31 (2014) 20–34.

[24] S. Dawlee, A. Jayakrishnan, M. Jayabalan, Studies on novel radiopaque methyl methacrylate: glycidyl methacrylate based polymer for biomedical applications, J. Mater. Sci – Mater. Med. 20 (2009) 243–250.

[25] S. Kiran, N.R. James, R. Joseph, A. Jayakrishnan, Synthesis and characterization of iodinated polyurethane with inherent radiopacity, Biomaterials 30 (2009) 5552–5559.

[26] M. Marcos, P. Cano, P. Fantazzini, C. Garavaglia, S. Gomez, L. Garrido, NMR relaxometry and imaging of water absorbed in biodegradable polymer scaffolds, Magn. Reson. Imaging 24 (2006) 89–95.

[27] F. Hallouard, S. Briancon, N. Anton, X. Li, T. Vandamme, H. Fessi, Influence of diblock copolymer PCL-mPEG and of various iodinated oils on the formulation by the emulsion–solvent diffusion process of radiopaque polymeric nanoparticles, J. Pharm. Sci. 102 (2013) 4150–4158.

[28] F. Hallouard, S. Briancon, N. Anton, X. Li, T. Vandamme, H. Fessi, Poly(ethylene glycol)-poly(epsilon-caprolactone) iodinated nanocapsules as contrast agents for X-ray imaging, Pharm. Res. 30 (2013) 2023–2035.

[29] F. Kiessling, S. Fokong, J. Bzyl, W. Lederle, M. Palmowski, T. Lammers, Recent advances in molecular, multimodal and theranostic ultrasound imaging, Adv. Drug Deliver. Rev. 72 (2014) 15–27.

[30] A. Raisinghani, A.N. DeMaria, Physical principles of microbubble ultrasound contrast agents, Am. J. Cardiol. 90 (2002) 3J–7J.

[31] M.R. Zalutsky, D.A. Reardon, O.R. Pozzi, G. Vaidyanathan, D.D. Bigner, Targeted alpha-particle radiotherapy with At-211-labeled monoclonal antibodies, Nucl. Med. Biol. 34 (2007) 779–785.

[32] T.J. Wadas, D.N. Pandya, K.K.S. Sai, A. Mintz, Molecular targeted alpha-particle therapy for oncologic applications, Am. J. Roentgenol. 203 (2014) 253–260.

[33] J.M. Idee, M. Port, I. Raynal, M. Schaefer, S. Le Greneur, C. Corot, Clinical and biological consequences of transmetallation induced by contrast agents for magnetic resonance imaging: a review, Fund. Clin. Pharmacol. 20 (2006) 563–576.

[34] T. Grobner, Gadolinium – a specific trigger for the development of nephrogenic fibrosing dermopathy and nephrogenic systemic fibrosis?, Nephrol Dial. Transpl. 21 (2006) 1104–1108.

[35] S.J. Lee, J.R. Jeong, S.C. Shin, J.C. Kim, Y.H. Chang, Y.M. Chang, J.D. Kim, Nanoparticles of magnetic ferric oxides encapsulated with poly(D,L latide-co-glycolide) and their applications to magnetic resonance imaging contrast agent, J. Magn. Magn. Mater. 272 (2004) 2432–2433.

[36] M.F. Bennewitz, T.L. Lobo, M.K. Nkansah, G. Ulas, G.W. Brudvig, E.M. Shapiro, Biocompatible and pH-sensitive PLGA encapsulated MnO nanocrystals for molecular and cellular MRI, ACS Nano 5 (2011) 3438–3446.

[37] Y. Wang, Y.W. Ng, Y. Chen, B. Shuter, J. Yi, J. Ding, S.-C. Wang, S.-S. Feng, Formulation of superparamagnetic iron oxides by nanoparticles of biodegradable polymers for magnetic resonance Imaging, Adv. Funct. Mater. 18 (2008) 308–318.

[38] Y.-C. Chen, W.-F. Lee, H.-H. Tsai, W.-Y. Hsieh, Paclitaxel and iron oxide loaded multifunctional nanoparticles for chemotherapy, fluorescence properties, and magnetic resonance imaging, J. Biomed. Mater. Res. A 100A (2012) 1279–1292.

[39] E.S. Lee, C. Lim, H.-T. Song, J.M. Yun, K.S. Lee, B.-J. Lee, Y.S. Youn, Y.T. Oh, K.T. Oh, A nanosized delivery system of superparamagnetic iron oxide for tumor MR imaging, Int. J. Pharm. 439 (2012) 342–348.

[40] C. Prashant, M. Dipak, C.-T. Yang, K.-H. Chuang, D. Jun, S.-S. Feng, Superparamagnetic iron oxide – loaded poly (lactic acid)-D-alpha-tocopherol polyethylene glycol 1000 succinate copolymer nanoparticles as MRI contrast agent, Biomaterials 31 (2010) 5588–5597.

[41] Y.F. Tan, P. Chandrasekharan, D. Maity, C.X. Yong, K.-H. Chuang, Y. Zhao, S. Wang, J. Ding, S.-S. Feng, Multimodal tumor imaging by iron oxides and quantum dots formulated in poly (lactic acid)-D-alpha-tocopheryl polyethylene glycol 1000 succinate nanoparticles, Biomaterials 32 (2011) 2969–2978.

[42] P.W. Lee, S.H. Hsu, J.S. Tsai, F.R. Chen, P.J. Huang, C.J. Ke, Z.X. Liao, C.W. Hsiao, H.J. Lin, H.W. Sung, Multifunctional core–shell polymeric nanoparticles for transdermal DNA delivery and epidermal Langerhans cells tracking, Biomaterials 31 (2010) 2425–2434.

[43] H. Wang, S. Wang, Z. Liao, P. Zhao, W. Su, R. Niu, J. Chang, Folate-targeting magnetic core–shell nanocarriers for selective drug release and imaging, Int. J. Pharm. 430 (2012) 342–349.

[44] L. Wang, K.-G. Neoh, E.-T. Kang, B. Shuter, S.-C. Wang, Biodegradable magnetic-fluorescent magnetite/poly(DL-lactic acid-co-alpha, beta-malic acid) composite nanoparticles for stem cell labeling, Biomaterials 31 (2010) 3502–3511.

[45] X. Gao, Y. Luo, Y. Wang, J. Pang, C. Liao, H. Lu, Y. Fang, Prostate stem cell antigen-targeted nanoparticles with dual functional properties: in vivo imaging and cancer chemotherapy, Int. J. Nanomed. 7 (2012) 4037–4051.

[46] Q. Wang, H. Su, C. Xia, J. Sun, C. Liu, Z. Wang, Q. Gong, B. Song, F. Gao, H. Ai, Z. Gu, Amphiphilic dextran/magnetite nanocomposites as magnetic resonance imaging probes, Chinese Sci. Bull. 54 (2009) 2925–2933.

[47] M. Filippousi, S.A. Papadimitriou, D.N. Bikiaris, E. Pavlidou, M. Angelakeris, D. Zamboulis, H. Tian, G. Van Tendeloo, Novel core–shell magnetic nanoparticles for Taxol encapsulation in biodegradable and biocompatible block copolymers: preparation, characterization and release properties, Int. J. Pharm. 448 (2013) 221–230.

[48] S. Mekkapat, B. Thong-On, B. Rutnakornpituk, U. Wichai, M. Rutnakornpituk, Magnetic core–bilayer shell complex of magnetite nanoparticle stabilized with mPEG-polyester amphiphilic block copolymer, J. Nanopart. Res. 15 (2013).

[49] H. Ai, C. Flask, B. Weinberg, X. Shuai, M.D. Pagel, D. Farrell, J. Duerk, J.M. Gao, Magnetite-loaded polymeric micelles as ultrasensitive magnetic-resonance probes, Adv. Mater. 17 (2005) 1949–1952.

[50] G.-B. Hong, J.-X. Zhou, R.-X. Yuan, Folate-targeted polymeric micelles loaded with ultrasmall superparamagnetic iron oxide: combined small size and high MRI sensitivity, Int. J. Nanomed. 7 (2012) 2863–2872.

[51] J. Lu, S. Ma, J. Sun, C. Xia, C. Liu, Z. Wang, X. Zhao, F. Gao, Q. Gong, B. Song, X. Shuai, H. Ai, Z. Gu, Manganese ferrite nanoparticle micellar nanocomposites as MRI contrast agent for liver imaging, Biomaterials 30 (2009) 2919–2928.

[52] D. Niu, X. Liu, Y. Li, Z. Ma, W. Dong, S. Chang, W. Zhao, J. Gu, S. Zhang, J. Shi, Fabrication of uniform, biocompatible and multifunctional PCL-*b*-PAA copolymer-based hybrid micelles for magnetic resonance imaging, J. Mater. Chem. 21 (2011) 13825–13831.

[53] D.-H. Kim, E.A. Vitol, J. Liu, S. Balasubramanian, D.J. Gosztola, E.E. Cohen, V. Novosad, E.A. Rozhkova, Stimuli-responsive magnetic nanomicelles as multifunctional heat and cargo delivery vehicles, Langmuir 29 (2013) 7425–7432.

[54] X. Xie, C. Zhang, Controllable assembly of hydrophobic superparamagnetic iron oxide nanoparticle with mPEG-PLA copolymer and its effect on MR transverse relaxation rate, J. Nanomater. (2011). ID 152524.

[55] N. Nasongkla, E. Bey, J. Ren, H. Ai, C. Khemtong, J. Guthi, S. Chin, A. Sherry, D. Boothman, J. Gao, Multifunctional polymeric micelles as cancer-targeted, MRI-ultrasensitive drug delivery systems, Nano Lett. 6 (2006) 2427–2430.

[56] X. Yang, J.J. Grailer, I.J. Rowland, A. Javadi, S.A. Hurley, D.A. Steeber, S. Gong, Multifunctional SPIO/DOX-loaded wormlike polymer vesicles for cancer therapy and MR imaging, Biomaterials 31 (2010) 9065–9073.

[57] B. Xu, R. Lu, H. Dou, K. Tao, K. Sun, Y. Qiu, J. Ding, D. Zhang, J. Li, W. Shi, K. Sun, Exploring the structure–property relationships of ultrasonic/MRI dual imaging magnetite/PLA microbubbles: magnetite@Cavity versus magnetite@Shell systems, Colloid Polym. Sci. 290 (2012) 1617–1626.

[58] F. Yang, A. Gu, Z. Chen, N. Gu, M. Ji, Multiple emulsion microbubbles for ultrasound imaging, Mater. Lett. 62 (2008) 121–124.

[59] B. Xu, H. Dou, K. Tao, K. Sun, J. Ding, W. Shi, X. Guo, J. Li, D. Zhang, K. Sun, "Two-in-One" Fabrication of Fe_3O_4/MePEG-PLA composite nanocapsules as a potential ultrasonic/MRI dual contrast agent, Langmuir 27 (2011) 12134–12142.

[60] A.Z. Faranesh, M.T. Nastley, C.P. de la Cruz, M.F. Haller, P. Laquerriere, K.W. Leong, E.R. McVeigh, In vitro release of vascular endothelial growth factor from gadolinium-doped biodegradable microspheres, Magn. Reson. Med. 51 (2004) 1265–1271.

[61] A.L. Doiron, K. Chu, A. Ali, L. Brannon-Peppas, Preparation and initial characterization of biodegradable particles containing gadolinium-DTPA contrast agent for enhanced MRI, P. Natl. Acad. Sci. USA 105 (2008) 17232–17237.

[62] A.L. Doiron, K.A. Homan, S. Emelianov, L. Brannon-Peppas, Poly(lactic-co-glycolic) acid as a carrier for imaging contrast agents, Pharm. Res. 26 (2009) 674–682.

[63] Z. Chen, D. Yu, S. Wang, N. Zhang, C. Ma, Z. Lu, Biocompatible nanocomplexes for molecular targeted MRI contrast agent, Nanoscale Res. Lett. 4 (2009) 618–626.

[64] G. Rigaux, V.G. Roullin, C. Cadiou, C. Portefaix, L. Van Gulick, G. Baeuf, M.C. Andry, C. Hoeffel, L.V. Elst, S. Laurent, R. Muller, M. Molinari, F. Chuburu, A new magnetic resonance imaging contrast agent loaded into poly(lacide-co-glycolide) nanoparticles for long-term detection of tumors, Nanotechnology 25 (2014).

[65] Z. Cheng, D.L.J. Thorek, A. Tsourkas, Porous polymersomes with encapsulated Gd-labeled dendrimers as highly efficient MRI contrast agents, Adv. Funct. Mater. 19 (2009) 3753–3759.

[66] Q. Liu, H. Zhu, J. Qin, H. Dong, J. Du, Theranostic vesicles based on bovine serum albumin and poly(ethylene glycol)-block-poly(L-lactic-co-glycolic acid) for magnetic resonance imaging and anticancer drug delivery, Biomacromolecules 15 (2014) 1586–1592.

[67] M. Ao, Z. Wang, H. Ran, D. Guo, J. Yu, A. Li, W. Chen, W. Wu, Y. Zheng, Gd-DTPA-loaded PLGA microbubbles as both ultrasound contrast agent and MRI contrast agent – a feasibility research, J. Biomed. Mater. Res. B 93B (2010) 551–556.

[68] M.F. Bennewitz, S.S. Williams, M.K. Nkansah, E.M. Shapiro, Poly(lactic-co-glycolic acid) encapsulated gadolinium oxide nanoparticles for MRI-based cell tracking, J. Nanosci. Nanotechnol. 13 (2013) 3778–3783.

[69] M. Srinivas, L.J. Cruz, F. Bonetto, A. Heerschap, C.G. Figdor, I.J.M. de Vries, Customizable, multi-functional fluorocarbon nanoparticles for quantitative in vivo imaging using F-19 MRI and optical imaging, Biomaterials 31 (2010) 7070–7077.

[70] O. Diou, E. Fattal, T. Payen, S.L. Bridal, J. Valette, N. Tsapis, Nanocapsules of perfluorooctyl bromide for theranostics: from formulation to targeting, Colloid. Nanoparticles Biomed. Appl. Ix 8955 (2014).

[71] O. Diou, N. Tsapis, C. Giraudeau, J. Valette, C. Gueutin, F. Bourasset, S. Zanna, C. Vauthier, E. Fattal, Long-circulating perfluorooctyl bromide nanocapsules for tumor imaging by (FMRI)-F-19, Biomaterials 33 (2012) 5593–5602.

[72] Y.-X. Wang, Superparamagnetic iron oxide based MRI contrast agents: current status of clinical application, Quant. Imaging Med. Surg. 1 (2011) 35–40.

[73] R.A. Wassel, B. Grady, R.D. Kopke, K.J. Dormer, Dispersion of super paramagnetic iron oxide nanoparticles in poly(D, L-lactide-co-glycolide) microparticles, Colloids Surf. A 292 (2007) 125–130.

[74] D. Patel, J.Y. Moon, Y. Chang, T.J. Kim, G.H. Lee, Poly(D, L-lactide-co-glycolide) coated superparamagnetic iron oxide nanoparticles: synthesis, characterization and in vivo study as MRI contrast agent, Colloids Surf. A 313 (2008) 91–94.

[75] T. Franklin-Ford, N. Shah, E. Leiferman, C.S. Chamberlain, A. Raval, R. Vanderby, W.L. Murphy, Tracking injectable microspheres in dynamic tissues with encapsulated superparamagnetic iron oxide nanoparticles, Macromol. Biosci. 12 (2012) 1615–1621.

[76] M.K. Nkansah, D. Thakral, E.M. Shapiro, Magnetic poly(lactide-co-glycolide) and cellulose particles for MRI-based cell tracking, Magn. Reson. Med. 65 (2011) 1776–1785.

[77] A. Akbarzadeh, H. Mikaeili, N. Zarghami, R. Mohammad, A. Barkhordari, S. Davaran, Preparation and in vitro evaluation of doxorubicin-loaded Fe3O4 magnetic nanoparticles modified with biocompatible copolymers, Int. J. Nanomed. 7 (2012) 511–526.

[78] M.F. Silva, A.A. Winkler Hechenleitner, D.M. Fernandes de Oliveira, M. Agueeros, R. Penalva, J. Manuel Irache, E.A. Gomez Pineda, Optimization of maghemite-loaded PLGA nanospheres for biomedical applications, Eur. J. Pharm. Sci. 49 (2013) 343–351.

[79] S. Aryal, J. Key, C. Stigliano, M.D. Landis, D.Y. Lee, P. Decuzzi, Positron emitting magnetic nanoconstructs for PET/MR imaging, Small 10 (2014) 2688–2696.

[80] J. Chen, A.Y. Sheu, W. Li, Z. Zhang, D.-H. Kim, R.J. Lewandowski, R.A. Omary, L.D. Shea, A.C. Larson, Poly(lactide-co-glycolide) microspheres for MRI-monitored transcatheter delivery of sorafenib to liver tumors, J. Control. Release 184 (2014) 10–17.

[81] F. Ye, A. Barrefelt, H. Asem, M. Abedi-Valugerdi, I. El-Serafi, M. Saghafian, K. Abu-Salah, S. Alrokayan, M. Muhammed, M. Hassan, Biodegradable polymeric vesicles containing magnetic nanoparticles, quantum dots and anticancer drugs for drug delivery and imaging, Biomaterials 35 (2014) 3885–3894.

[82] Y. Ling, K. Wei, F. Zou, S. Zhong, Temozolomide loaded PLGA-based superparamagnetic nanoparticles for magnetic resonance imaging and treatment of malignant glioma, Int. J. Pharm. 430 (2012) 266–275.

[83] A. Yakar, G. Tansik, T. Keskin, U. Gunduz, Tailoring the magnetic behavior of polymeric particles for bioapplications, J. Polym. Eng. 33 (2013) 265–274.

[84] M. Hamoudeh, H. Fessi, Preparation, characterization and surface study of poly-epsilon caprolactone magnetic microparticles, J. Colloid Interf. Sci. 300 (2006) 584–590.

[85] D. Cheng, G. Hong, W. Wang, R. Yuan, H. Ai, J. Shen, B. Liang, J. Gao, X. Shuai, Nonclustered magnetite nanoparticle encapsulated biodegradable polymeric micelles with enhanced properties for in vivo tumor imaging, J. Mater. Chem. 21 (2011) 4796–4804.

[86] R.N. Mariano, D. Alberti, J.C. Cutrin, S.G. Crich, S. Aime, Design of PLGA based nanoparticles for imaging guided applications, Mol. Pharm. 11 (2014) 4100–4106.

[87] C. Zheng, M. Zheng, P. Gong, D. Jia, P. Zhang, B. Shi, Z. Sheng, Y. Ma, L. Cai, Indocyanine green-loaded biodegradable tumor targeting nanoprobes for in vitro and in vivo imaging, Biomaterials 33 (2012) 5603–5609.

[88] B. Sitharaman, M. Van Der Zande, J.S. Ananta, X. Shi, A. Veltien, X.F. Walboomers, L.J. Wilson, A.G. Mikos, A. Heerschap, J.A. Jansen, Magnetic resonance imaging studies on gadonanotube-reinforced biodegradable polymer nanocomposites, J. Biomed. Mater. Res. A 93A (2010) 1454–1462.

[89] O. Diou, E. Fattal, V. Delplace, N. Mackiewicz, J. Nicolas, S. Meriaux, J. Valette, C. Robic, N. Tsapis, RGD decoration of PEGylated polyester nanocapsules of perfluorooctyl bromide for tumor imaging: influence of pre or post-functionalization on capsule morphology, Eur. J. Pharm. Biopharm. 87 (2014) 170–177.

[90] H. Kobayashi, M. Ogawa, R. Alford, P.L. Choyke, Y. Urano, New strategies for fluorescent probe design in medical diagnostic imaging, Chem. Rev. 110 (2010) 2620–2640.
[91] J. Panyam, S.K. Sahoo, S. Prabha, T. Bargar, V. Labhasetwar, Fluorescence and electron microscopy probes for cellular and tissue uptake of poly(D, L-lactide-co-glycolide) nanoparticles, Int. J. Pharm. 262 (2003) 1–11.
[92] G. Tosi, F. Rivasi, F. Gandolfi, L. Costantino, M.A. Vandelli, F. Forni, Conjugated poly(D, L-lactide-co-glycolide) for the preparation of in vivo detectable nanoparticles, Biomaterials 26 (2005) 4189–4195.
[93] M. Gaumet, R. Gurny, F. Delie, Fluorescent biodegradable PLGA particles with narrow size distributions: preparation by means of selective centrifugation, Int. J. Pharm. 342 (2007) 222–230.
[94] G. Tosi, L. Costantino, F. Rivasi, B. Ruozi, E. Leo, A.V. Vergoni, R. Tacchi, A. Bertolini, M.A. Vandelli, F. Forni, Targeting the central nervous system: in vivo experiments with peptide-derivatized nanoparticles loaded with Loperamide and Rhodamine-123, J. Control. Release 122 (2007) 1–9.
[95] F.-Y. Cheng, S.P.-H. Wang, C.-H. Su, T.-L. Tsai, P.-C. Wu, D.-B. Shieh, J.-H. Chen, P.C.-H. Hsieh, C.-S. Yeh, Stabilizer-free poly(lactide-co-glycolide) nanoparticles for multimodal biomedical probes, Biomaterials 29 (2008) 2104–2112.
[96] M. Kolitz-Domb, I. Grinberg, E. Corem-Salkmon, S. Margel, Engineering of near infrared fluorescent proteinoid-poly(L-lactic acid) particles for in vivo colon cancer detection, J. Nanobiotechnol. 12 (30) (2014) 1–13.
[97] H. Cho, G.L. Indig, J. Weichert, H.-C. Shin, G.S. Kwon, In vivo cancer imaging by poly(ethylene glycol)-b-poly(epsilon-caprolactone) micelles containing a near-infrared probe, Nanomed. – Nanotechnol. 8 (2012) 228–236.
[98] I.L. Medintz, H.T. Uyeda, E.R. Goldman, H. Mattoussi, Quantum dot bioconjugates for imaging, labelling and sensing, Nat. Mater. 4 (2005) 435–446.
[99] X. Michalet, F.F. Pinaud, L.A. Bentolila, J.M. Tsay, S. Doose, J.J. Li, G. Sundaresan, A.M. Wu, S.S. Gambhir, S. Weiss, Quantum dots for live cells, in vivo imaging, and diagnostics, Science 307 (2005) 538–544.
[100] Y. Nagasaki, T. Ishii, Y. Sunaga, Y. Watanabe, H. Otsuka, K. Kataoka, Novel molecular recognition via fluorescent resonance energy transfer using a biotin-PEG/polyamine stabilized CdS quantum dot, Langmuir 20 (2004) 6396–6400.
[101] B. Dubertret, P. Skourides, D.J. Norris, V. Noireaux, A.H. Brivanlou, A. Libchaber, In vivo imaging of quantum dots encapsulated in phospholipid micelles, Science 298 (2002) 1759–1762.
[102] G.N. Guo, W. Liu, J.G. Liang, H.B. Xu, Z.K. He, X.L. Yang, Preparation and characterization of novel CdSe quantum dots modified with poly(D, L-lactide) nanoparticles, Mater. Lett. 60 (2006) 2565–2568.
[103] B.J. Nehilla, P.G. Allen, T.A. Desai, Surfactant-free, drug-quantum-dot coloaded poly(lactide-co-glycolide) nanoparticles: towards multifunctional nanoparticles, ACS Nano 2 (2008) 538–544.
[104] J. Pan, Y. Wang, S.-S. Feng, Formulation, characterization, and in vitro evaluation of quantum dots loaded in poly(lactide)-vitamin E TPGS nanoparticles for cellular and molecular imaging, Biotechnol. Bioeng. 101 (2008) 622–633.
[105] X.D. Hou, Q.B. Li, L. Jia, Y. Li, Y.D. Zhu, A.M. Cao, New preparation of structurally symmetric, biodegradable poly(L-lactide) disulfides and PLLA-stabilized, photoluminescent CdSe quantum dots, Macromol. Biosci. 9 (2009) 551–562.
[106] W.S. Kuo, Y.C. Ku, H.T. Sei, F.Y. Cheng, C.S. Yeh, Paclitaxel-loaded stabilizer-free poly(D, L-lactide-co-glycolide) nanoparticles conjugated with quantum dots for reversion of anti-cancer drug resistance and cancer cellular imaging, J. Chin. Chem. Soc. – TAIP 56 (2009) 923–934.
[107] J. Pan, S.-S. Feng, Targeting and imaging cancer cells by Folate-decorated, quantum dots (QDs)-loaded nanoparticles of biodegradable polymers, Biomaterials 30 (2009) 1176–1183.
[108] C.H. Yang, K.S. Huang, Y.S. Lin, K. Lu, C.C. Tzeng, E.C. Wang, C.H. Lin, W.Y. Hsu, J.Y. Chang, Microfluidic assisted synthesis of multi-functional polycaprolactone microcapsules: incorporation of CdTe quantum dots, Fe_3O_4 superparamagnetic nanoparticles and tamoxifen anticancer drugs, Lab Chip 9 (2009) 961–965.
[109] J.S. Kim, K.J. Cho, T.H. Tran, M. Nurunnabi, T.H. Moon, S.M. Hong, Y.-K. Lee, In vivo NIR imaging with CdTe/CdSe quantum dots entrapped in PLGA nanospheres, J. Colloid Interf. Sci. 353 (2011) 363–371.
[110] G.Y. Liu, X.S. Liu, S.S. Wang, C.J. Chen, J. Ji, Biomimetic polymersomes as carriers for hydrophilic quantum dots, Langmuir 28 (2012) 557–562.
[111] T. Endres, M. Zheng, A. Kilic, A. Turowska, M. Beck-Broichsitter, H. Renz, O.M. Merkel, T. Kissel, Amphiphilic biodegradable PEG-PCL-PEI triblock copolymers for FRET-capable in vitro and in vivo delivery of siRNA and quantum dots, Mol. Pharm. 11 (2014) 1273–1281.
[112] J. Nicolas, D. Brambilla, O. Carion, T. Pons, I. Maksimovic, E. Larquet, B. Le Droumaguet, K. Andrieux, B. Dubertret, P. Couvreur, Quantum dot-loaded PEGylated poly(alkyl cyanoacrylate) nanoparticles for in vitro and in vivo imaging, Soft Matter 7 (2011) 6187–6193.
[113] F. Zhang, E. Lees, F. Amin, P.R. Gil, F. Yang, P. Mulvaney, W.J. Parak, Polymer-coated nanoparticles: a universal tool for biolabelling experiments, Small 7 (2011) 3113–3127.
[114] A. El-Batta, H.A. Al-Muallem, M.N. Shaikh, N. Maalej, Polymer nanoparticles containing 2,4,6-triiodophenol: a potential contrast medium for medical imaging, Acta Chim. Slov. 61 (2014) 414–419.
[115] A. Jakhmola, N. Anton, H. Anton, N. Messaddeq, F. Hallouard, A. Klymchenko, Y. Mely, T.F. Vandamme, Poly-epsilon-caprolactone tungsten oxide nanoparticles as a contrast agent for X-ray computed tomography, Biomaterials 35 (2014) 2981–2986.
[116] D.M. El-Sherif, M.A. Wheatley, Development of a novel method for synthesis of a polymeric ultrasound contrast agent, J. Biomed. Mater. Res. A 66A (2003) 347–355.
[117] J.M. Correas, L. Bridal, A. Lesavre, A. Mejean, M. Claudon, O. Helenon, Ultrasound contrast agents: properties, principles of action, tolerance, and artifacts, Eur. Radiol. 11 (2001) 1316–1328.
[118] A.L. Klibanov, Ultrasound molecular imaging with targeted microbubble contrast agents, J. Nucl. Cardiol. 14 (2007) 876–884.
[119] J.A. Straub, D.E. Chickering, C.C. Church, B. Shah, T. Hanlon, H. Bernstein, Porous PLGA microparticles: AI-700, an intravenously administered ultrasound contrast agent for use in echocardiography, J. Control. Release 108 (2005) 21–32.
[120] J.D. Lathia, L. Leodore, M.A. Wheatley, Polymeric contrast agent with targeting potential, Ultrasonics 42 (2004) 763–768.
[121] E. Pisani, N. Tsapis, B. Galaz, M. Santin, R. Berti, N. Taulier, E. Kurtisovski, O. Lucidarme, M. Ourevitch, B.T. Doan, J.C. Beloeil, B. Gillet, W. Urbach, S.L. Bridal, E. Fattal, Perfluorooctyl bromide polymeric capsules as dual contrast agents for ultrasonography and magnetic resonance imaging, Adv. Funct. Mater. 18 (2008) 2963–2971.
[122] J.R. Lindner, Microbubbles in medical imaging: current applications and future directions, Nat. Rev. Drug Discov. 3 (2004) 527–532.
[123] J. Liu, J. Li, T.J. Rosol, X. Pan, J.L. Voorhees, Biodegradable nanoparticles for targeted ultrasound imaging of breast cancer cells in vitro, Phys. Med. Biol. 52 (2007) 4739–4747.
[124] R. Diaz-Lopez, N. Tsapis, D. Libong, P. Chaminade, C. Connan, M.M. Chehimi, R. Berti, N. Taulier, W. Urbach, V. Nicolas, E. Fattal, Phospholipid decoration of microcapsules containing perfluorooctyl bromide used as ultrasound contrast agents, Biomaterials 30 (2009) 1462–1472.
[125] B. Liu, X. Zhou, F. Yang, H. Shen, S. Wang, B. Zhang, G. Zhi, D. Wu, Fabrication of uniform sized polylactone microcapsules by premix membrane emulsification for ultrasound imaging, Polym. Chem. 5 (2014) 1693–1701.
[126] J.R. Eisenbrey, O.M. Burstein, R. Kambhampati, F. Forsberg, J.B. Liu, M.A. Wheatley, Development and optimization of a doxorubicin loaded poly(lactic acid) contrast agent for ultrasound directed drug delivery, J. Control. Release 143 (2010) 38–44.
[127] J. Ma, L.X. Xing, M. Shen, F. Li, M.J. Zhu, L.F. Jin, Z. Li, F. Gao, Y. Su, Y.R. Duan, L.F. Du, Ultrasound contrast-enhanced imaging and in vitro antitumor effect of paclitaxel-poly(lactic-co-glycolic acid)-monomethoxypoly (ethylene glycol) nanocapsules with ultrasound-targeted microbubble destruction, Mol. Med. Rep. 11 (2015) 2413–2420.
[128] Z.W. Bai, R.X. Zhuo, Synthesis and characterization of polyester Gd(III) complexes, Acta Polym. Sin. (1998) 191–195.
[129] I. Pashkunova-Martic, C. Kremser, M. Galanski, P. Schluga, V. Arion, P. Debbage, W. Jaschke, B. Keppler, Lectin conjugates as biospecific contrast agents for MRI. Coupling of *Lycopersicon esculentum* agglutinin to linear water-soluble DTPA-loaded oligomers, Mol. Imaging Biol. 13 (2011) 432–442.
[130] K.C. Yu, H.B. Hu, M.L. Liu, H.Z. Yuan, C.H. Ye, R.X. Zhuo, NMR relaxivity and imaging of neutral macromolecular polyester gadolinium (III) complexes, Chinese J. Polym. Sci. 17 (1999) 471–475.
[131] G.P. Yan, R.X. Zhuo, M.Y. Xu, X. Zhang, L.Y. Li, Hepatic targeting of macromolecular MRI contrast agents, Polym. Int. 51 (2002) 892–898.
[132] X.J. Li, Y.F. Qian, T. Liu, X.L. Hu, G.Y. Zhang, Y.Z. You, S.Y. Liu, Amphiphilic multiarm star block copolymer-based multifunctional unimolecular micelles for cancer targeted drug delivery and MR imaging, Biomaterials 32 (2011) 6595–6605.
[133] Z. Sideratou, D. Tsiourvas, T. Theodossiou, M. Fardis, C.M. Paleos, Synthesis and characterization of multifunctional hyperbranched polyesters as prospective contrast agents for targeted MRI, Bioorg. Med. Chem. Lett. 20 (2010) 4177–4181.
[134] T. Liu, Y. Qian, X. Hu, Z. Ge, S. Liu, Mixed polymeric micelles as multifunctional scaffold for combined magnetic resonance imaging contrast enhancement and targeted chemotherapeutic drug delivery, J. Mater. Chem. 22 (2012) 5020–5030.
[135] K.S. Kim, W. Park, J. Hu, Y.H. Bae, K. Na, A cancer-recognizable MRI contrast agents using pH-responsive polymeric micelle, Biomaterials 35 (2014) 337–343.
[136] M. Ye, Y. Qian, J. Tang, H. Hu, M. Sui, Y. Shen, Targeted biodegradable dendritic MRI contrast agent for enhanced tumor imaging, J. Control. Release 169 (2013) 239–245.
[137] M. Ye, Y. Qian, Y. Shen, H. Hu, M. Sui, J. Tang, Facile synthesis and in vivo evaluation of biodegradable dendritic MRI contrast agents, J. Mater. Chem. 22 (2012) 14369–14377.
[138] T. Li, Y. Qian, M. Ye, J. Tang, H. Hu, Y. Shen, Synthesis and properties of a biodegradable dendritic magnetic resonance imaging contrast agent, Chinese J. Chem. 32 (2014) 91–96.
[139] M. Grogna, R. Cloots, A. Luxen, C. Jerome, C. Passirani, N. Lautram, J.-F. Desreux, C. Detrembleur, Polymer micelles decorated by gadolinium complexes as MRI blood contrast agents: design, synthesis and properties, Polym. Chem. 1 (2010) 1485–1490.
[140] X.-M. Sun, J.-X. Xu, J.-B. Tang, M.-H. Sui, Y.-Q. Shen, Folate-targeted optical and magnetic resonance dualmodality PCL-b-PEG micelles for tumor imaging, Chinese J. Polym. Sci. 29 (2011) 427–430.

[141] Z. Chen, D. Yu, C. Liu, X. Yang, N. Zhang, C. Ma, J. Song, Z. Lu, Gadolinium-conjugated PLA-PEG nanoparticles as liver targeted molecular MRI contrast agent, J. Drug Target. 19 (2011) 657–665.
[142] G. Zhang, R. Zhang, X. Wen, L. Li, C. Li, Micelles based on biodegradable poly(L-glutamic acid)-b-polylactide with paramagnetic Gd ions chelated to the shell layer as a potential nanoscale IVIRI-visible delivery system, Biomacromolecules 9 (2008) 36–42.
[143] S. Blanquer, O. Guillaume, V. Letouzey, L. Lemaire, F. Franconi, C. Paniagua, J. Coudane, X. Garric, New magnetic-resonance-imaging-visible poly(ε-caprolactone)-based polyester for biomedical applications, Acta Biomater. 8 (2012) 1339–1347.
[144] Y. Li, S. Laurent, L. Esser, L.V. Elst, R.N. Muller, A.B. Lowe, C. Boyer, T.P. Davis, The precise molecular location of gadolinium atoms has a significant influence on the efficacy of nanoparticulate MRI positive contrast agents, Polym. Chem. 5 (2014) 2592–2601.
[145] S. El Habnouni, B. Nottelet, V. Darcos, B. Porsio, L. Lemaire, F. Franconi, X. Garric, J. Coudane, MRI-visible poly(ε-caprolactone) with controlled contrast agent ratios for enhanced visualization in temporary imaging applications, Biomacromolecules 14 (2013) 3626–3634.
[146] L. Jing, X. Liang, X. Li, Y. Yang, Z. Dai, Covalent attachment of Mn-porphyrin onto doxorubicin-loaded poly(lactic acid) nanoparticles for potential magnetic resonance imaging and pH-sensitive drug delivery, Acta Biomater. 9 (2013) 9434–9441.
[147] G. Ratzinger, P. Agrawal, W. Koerner, J. Lonkai, H.M.H.F. Sanders, E. Terreno, M. Wirth, G.J. Strijkers, K. Nicolay, F. Gabor, Surface modification of PLGA nanospheres with Gd-DTPA and Gd-DOTA for high-relaxivity MRI contrast agents, Biomaterials 31 (2010) 8716–8723.
[148] H. Xie, S. Poyraz, M. Thu, Y. Liu, E.Y. Snyder, J.W. Smith, X. Zhang, Microwave-assisted fabrication of carbon nanotubes decorated polymeric nano-medical platforms for simultaneous drug delivery and magnetic resonance imaging, RSC Adv. 4 (2014) 5649–5652.
[149] G. Zhang, J. Chen, S.J. Payne, S.E. Kooi, J.N. Demas, C.L. Fraser, Multi-emissive difluoroboron dibenzoylmethane polylactide exhibiting intense fluorescence and oxygen-sensitive room-temperature phosphorescence, J. Am. Chem. Soc. 129 (2007) 8942–8943.
[150] A. Pfister, G. Zhang, J. Zareno, A.F. Horwitz, C.L. Fraser, Boron polylactide nanoparticles exhibiting fluorescence and phosphorescence in aqueous medium, ACS Nano 2 (2008) 1252–1258.
[151] C.A. Nguyen, E. Allemann, G. Schwach, E. Doelker, R. Gurny, Synthesis of a novel fluorescent poly(D, L-lactide) end-capped with 1-pyrenebutanol used for the preparation of nanoparticles, Eur. J. Pharm. Sci. 20 (2003) 217–222.
[152] H.H. Chen, R. Anbarasan, L.S. Kuo, P.H. Chen, Synthesis and characterizations of novel acid functionalized and fluorescent poly(ε-caprolactone), J. Mater. Sci. 46 (2011) 1796–1805.
[153] H.A. Klok, S. Becker, F. Schuch, T. Pakula, K. Mullen, Synthesis and solid state properties of novel fluorescent polyester star polymers, Macromol. Biosci. 3 (2003) 729–741.
[154] R. Reul, N. Tsapis, H. Hillaireau, L. Sancey, S. Mura, M. Recher, J. Nicolas, J.-L. Coll, E. Fattal, Near infrared labeling of PLGA for in vivo imaging of nanoparticles, Polym. Chem. 3 (2012) 694–702.
[155] N. Mackiewicz, J. Nicolas, N. Handke, M. Noiray, J. Mougin, C. Daveu, H.R. Lakkireddy, D. Bazile, P. Couvreur, Precise engineering of multifunctional PEGylated polyester nanoparticles for cancer cell targeting and imaging, Chem. Mater. 26 (2014) 1834–1847.
[156] H. Freichels, F. Danhier, V. Preat, P. Lecomte, C. Jerome, Fluorescent labeling of degradable poly(lactide-co-glycolide) for cellular nanoparticles tracking in living cells, Int. J. Artif. Organs 34 (2011) 152–160.
[157] K.Y. Peng, S.W. Wang, M.Y. Hua, R.S. Lee, Methoxy poly(ethylene glycol)-b-poly(ε-caprolactone) block-graft copolymers with pendant fluorescent groups: synthesis, characterization and cellular uptake, J. Polym. Res. 20 (62) (2013) 1–10.
[158] S.H. Kim, J.H. Jeong, K.W. Chun, T.G. Park, Target-specific cellular uptake of PLGA nanoparticles coated with poly(L-lysine)-poly(ethylene glycol)-folate conjugate, Langmuir 21 (2005) 8852–8857.
[159] Y.I. Chung, J.C. Kim, Y.H. Kim, G. Tae, S.Y. Lee, K. Kim, I.C. Kwon, The effect of surface functionalization of PLGA nanoparticles by heparin- or chitosan-conjugated Pluronic on tumor targeting, J. Control. Release 143 (2010) 374–382.
[160] W.X. Xi, T.F. Scott, C.J. Kloxin, C.N. Bowman, Click chemistry in materials science, Adv. Funct. Mater. 24 (2014) 2572–2590.
[161] V. Kaplun, D. Stepensky, Efficient decoration of nanoparticles intended for intracellular drug targeting with targeting residues, as revealed by a new indirect analytical approach, Mol. Pharm. 11 (2014) 2906–2914.
[162] S. El Habnouni, V. Darcos, X. Garric, J.P. Lavigne, B. Nottelet, J. Coudane, Mild methodology for the versatile chemical modification of polylactide surfaces: original combination of anionic and click chemistry for biomedical applications, Adv. Funct. Mater. 21 (2011) 3321–3330.
[163] C. Sardo, B. Nottelet, D. Triolo, G. Giammona, X. Garric, J.P. Lavigne, G. Cavallaro, J. Coudane, When functionalization of PLA surfaces meets thiol-yne photochemistry: case study with antibacterial polyaspartamide derivatives, Biomacromolecules 15 (2014) 4351–4362.
[164] B.C. Thanoo, M.C. Sunny, A. Jayakrishnan, Tantalum-loaded polyurethane microspheres for particulate embolization – preparation and properties, Biomaterials 12 (1991) 525–528.
[165] B.C. Thanoo, A. Jayakrishnan, Barium sulfate-loaded P(Hema) microspheres as artificial emboli – preparation and properties, Biomaterials 11 (1990) 477–481.
[166] F. Luderer, I. Begerow, W. Schmidt, H. Martin, N. Grabow, C.M. Buenger, W. Schareck, K.-P. Schmitz, K. Sternberg, Enhanced visualization of biodegradable polymeric vascular scaffolds by incorporation of gold, silver and magnetite nanoparticles, J. Biomater. Appl. 28 (2013) 219–231.
[167] C. Shasteen, S.M. Kwon, K.Y. Park, S.Y. Jung, S.H. Lee, C.G. Park, M.H. Kim, S. Kim, W.-C. Son, T.H. Choi, Y.B. Choy, Biodegradable internal fixation plates enabled with X-ray visibility by a radiopaque layer of beta-tricalcium phosphate and poly (lactic-co-glycolic acid), J. Biomed. Mater. Res. B 101B (2013) 320–329.
[168] T. Lamsa, H. Jin, J. Mikkonen, J. Laukkarinen, J. Sand, I. Nordback, Biocompatibility of a new bioabsorbable radiopaque stent material ($BaSO_4$ containing poly-L, D-lactide) in the rat pancreas, Pancreatology 6 (2006) 301–305.
[169] I. Nordback, S. Raty, J. Laukkarinen, S. Jarvinen, A. Piironen, J. Leppiniemi, M. Kellomaki, J. Sand, A novel radiopaque biodegradable stent for pancreatobiliary applications – the first human phase I trial in the pancreas, Pancreatology 12 (2012) 264–271.
[170] L. Mazzocchetti, M. Scandola, A. Pollicino, Study of the organic–inorganic phase interactions in polyester–titania hybrids, Polymer 49 (2008) 5215–5224.
[171] L. Mazzocchetti, E. Cortecchia, M. Scandola, Organic–inorganic hybrids as transparent coatings for UV and X-ray shielding, ACS Appl. Mater. Interf. 1 (2009) 726–734.
[172] J.L. Pariente, L. Bordenave, R. Bareille, C. Ohayon-Courtes, C. Baquey, M. Le Guillou, In vitro cytocompatibility of radio-opacifiers used in ureteral endoprosthesis, Biomaterials 20 (1999) 523–527.
[173] D. Mawad, H. Mouaziz, A. Penciu, H. Mehier, B. Fenet, H. Fessi, Y. Chevalier, Elaboration of radiopaque iodinated nanoparticles for in situ control of local drug delivery, Biomaterials 30 (2009) 5667–5674.
[174] F. Mottu, D.A. Rufenacht, A. Laurent, E. Doelker, Iodine-containing cellulose mixed esters as radiopaque polymers for direct embolization of cerebral aneurysms and arteriovenous malformations, Biomaterials 23 (2002) 121–131.
[175] A. Galperin, S. Margel, Synthesis and characterization of new micrometer-sized radiopaque polymeric particles of narrow size distribution by a single-step swelling of uniform polystyrene template microspheres for X-ray imaging applications, Biomacromolecules 7 (2006) 2650–2660.
[176] N.R. James, J. Philip, A. Jayakrishnan, Polyurethanes with radiopaque properties, Biomaterials 27 (2006) 160–166.
[177] M.A.B. Kruft, A. Benzina, F. Bar, F.H. Vanderveen, C.W.M. Bastiaansen, R. Blezer, T. Lindhout, L.H. Koole, Studies on two new radiopaque polymeric biomaterials, J. Biomed. Mater. Res. 28 (1994) 1259–1266.
[178] M.A.B. Kruft, A. Benzina, R. Blezer, L.H. Koole, Studies on radio-opaque polymeric biomaterials with potential applications to endovascular prostheses, Biomaterials 17 (1996) 1803–1812.
[179] M.A.B. Kruft, L.H. Koole, A convenient method to measure monomer reactivity ratios. Application to synthesis of polymeric biomaterials featuring intrinsic radiopacity, Macromolecules 29 (1996) 5513–5519.
[180] E.J.H. Boelen, G. Lewis, J. Xu, T. Slots, L.H. Koole, C.S.J. van Hooy-Corstjens, Evaluation of a highly-radiopaque iodine-containing acrylic bone cement for use in augmentation of vertebral compression fractures, J. Biomed. Mater. Res. A 86A (2008) 76–88.
[181] N. Moszner, U. Salz, A.M. Klester, V. Rheinberger, Synthesis and polymerization of hydrophobic iodine-containing methacrylates, Angew. Makromol. Chem. 224 (1995) 115–123.
[182] C. Zaharia, T. Zecheru, M.F. Moreau, F. Pascaretti-Grizon, G. Mabilleau, B. Marculescu, R. Filmon, C. Cincu, G. Staikos, D. Chappard, Chemical structure of methylmethacrylate-2-[2′,3′,5′-triiodobenzoyl] oxoethyl methacrylate copolymer, radio-opacity, in vitro and in vivo biocompatibility, Acta Biomater. 4 (2008) 1762–1769.
[183] A. Benzina, M.A.B. Kruft, F.H. vanderVeen, F.H.M.W. Bar, R. Blezer, T. Lindhout, L.H. Koole, A versatile three-iodine molecular building block leading to new radiopaque polymeric biomaterials, J. Biomed. Mater. Res. 32 (1996) 459–466.
[184] D. Horak, M. Metalova, F. Rypacek, New radiopaque polyHEMA-based hydrogel particles, J. Biomed. Mater. Res. 34 (1997) 183–188.
[185] B. Vazquez, M.P. Ginebra, F.J. Gil, J.A. Planell, A.L. Bravo, J. San Roman, Radiopaque acrylic cements prepared with a new acrylic derivative of iodo-quinoline, Biomaterials 20 (1999) 2047–2053.
[186] K. Saralidze, Y.B.J. Aldenhoff, M.L.W. Knetsch, L.H. Koole, Injectable polymeric microspheres with X-ray visibility. Preparation, properties, and potential utility as new traceable bulking agents, Biomacromolecules 4 (2003) 793–798.
[187] M.D. Hindenlang, A.A. Soudakov, G.H. Imler, C.T. Laurencin, L.S. Nair, H.R. Allcock, Iodine-containing radio-opaque polyphosphazenes, Polym. Chem. 1 (2010) 1467–1474.
[188] K.A. Aamer, K.L. Genson, J. Kohn, M.L. Becker, Impact of polymer-bound iodine on fibronectin adsorption and osteoblast cell morphology in radiopaque medical polymers: tyrosine-derived polycarbonate blends as a model system, Biomacromolecules 10 (2009) 2418–2426.
[189] W. Wang, J. Liu, C. Li, J. Zhang, J. Liu, A. Dong, D. Kong, Real-time and non-invasive fluorescence tracking of in vivo degradation of the thermosensitive PEGlyated polyester hydrogel, J. Mater. Chem. B 2 (2014) 4185–4192.
[190] B. Nottelet, J. Coudane, M. Vert, Synthesis of an X-ray opaque biodegradable copolyester by chemical modification of poly (ε-caprolactone), Biomaterials 27 (2006) 4948–4954.

[191] S. El Habnouni, S. Blanquer, V. Darcos, J. Coudane, Aminated PCL-based copolymers by chemical modification of poly(alpha-iodo-epsilon-caprolactone-co-epsilon-caprolactone), J. Polym. Sci. Polym. Chem. 47 (2009) 6104–6115.
[192] S. El Habnouni, V. Darcos, J. Coudane, Synthesis and ring opening polymerization of a new functional lactone, alpha-iodo-epsilon-caprolactone: a novel route to functionalized aliphatic polyesters, Macromol. Rapid Commun. 30 (2009) 165–169.
[193] C. Rode, A. Schmidt, R. Wyrwa, J. Weisser, K. Schmidt, N. Moszner, R.P. Gottlober, K. Heinemann, M. Schnabelrauch, Synthesis and processability into textile structures of radiopaque, biodegradable polyesters and poly(ester-urethanes), Polym. Int. 63 (2014) 1732–1740.
[194] A.L. Carbone, M. Song, K.E. Uhrich, Iodinated salicylate-based poly(anhydride-esters) as radiopaque biomaterials, Biomacromolecules 9 (2008) 1604–1612.
[195] K. Saatchi, U.O. Haefeli, Radiolabeling of biodegradable polymeric microspheres with Tc-99m(CO)(3) (+) and in vivo biodistribution evaluation using microSPECT/CT imaging, Bioconjugate Chem. 20 (2009) 1209–1217.
[196] L. Sang, Z.Y. Wei, K.L. Liu, X.H. Wang, K.D. Song, H. Wang, M. Qi, Biodegradable radiopaque iodinated poly(ester urethane)s containing poly(ε-caprolactone) blocks: synthesis, characterization, and biocompatibility, J. Biomed. Mater. Res. A 102 (2014) 1121–1130.
[197] S. Ponsart, J. Coudane, J.L. Morgat, M. Vert, Synthesis of H-3 and fluorescence-labelled poly (DL-lactic acid), J. Labelled Compd. Rad. 44 (2001) 677–687.
[198] M.C. Parrott, S.R. Benhabbour, C. Saab, J.A. Lemon, S. Parker, J.F. Valliant, A. Adronov, Synthesis, radiolabeling, and bio-imaging of high-generation polyester dendrimers, J. Am. Chem. Soc. 131 (2009) 2906–2916.
[199] B. Hoang, H. Lee, R.M. Reilly, C. Allen, Noninvasive monitoring of the fate of In-111-labeled block copolymer micelles by high resolution and high sensitivity microSPECT/CT imaging, Mol. Pharm. 6 (2009) 581–592.
[200] P.L. Lu, Y.C. Chen, T.W. Ou, H.H. Chen, H.C. Tsai, C.J. Wen, C.L. Lo, S.P. Wey, K.J. Lin, T.C. Yen, G.H. Hsiue, Multifunctional hollow nanoparticles based on graft-diblock copolymers for doxorubicin delivery, Biomaterials 32 (2011) 2213–2221.
[201] J. Guo, H. Hong, G. Chen, S. Shi, Q. Zheng, Y. Zhang, C.P. Theuer, T.E. Barnhart, W. Cai, S. Gong, Image-guided and tumor-targeted drug delivery with radiolabeled unimolecular micelles, Biomaterials 34 (2013) 8323–8332.
[202] J. Guo, H. Hong, G. Chen, S. Shi, T.R. Nayak, C.P. Theuer, T.E. Barnhart, W. Cai, S. Gong, Theranostic unimolecular micelles based on brush-shaped amphiphilic block copolymers for tumor-targeted drug delivery and positron emission tomography imaging, ACS Appl. Mater. Interf. 6 (2014) 21769–21779.
[203] R.W. Sirianni, M.-Q. Zheng, T.R. Patel, T. Shafbauer, J. Zhou, W.M. Saltzman, R.E. Carson, Y. Huang, Radiolabeling of poly(lactic-co-glycolic acid) (PLGA) nanoparticles with biotinylated F-18 prosthetic groups and imaging of their delivery to the brain with positron emission tomography, Bioconjugate Chem. 25 (2014) 2157–2165.
[204] E.T. Ahrens, J.W.M. Bulte, Tracking immune cells in vivo using magnetic resonance imaging, Nat. Rev. Immunol. 13 (2013) 755–763.
[205] D. Granot, M.K. Nkansah, M.F. Bennewitz, K.S. Tang, E.A. Markakis, E.M. Shapiro, Clinically viable magnetic poly(lactide-co-glycolide) particles for MRI-based cell tracking, Magn. Reson. Med. 71 (2014) 1238–1250.
[206] A. Preda, M. van Vliet, G.P. Krestin, R.C. Brasch, C.F. van Dijke, Magnetic resonance macromolecular agents for monitoring tumor microvessels and angiogenesis inhibition, Invest. Radiol. 41 (2006) 325–331.
[207] J. Zhou, D. Guo, Y. Zhang, W. Wu, H. Ran, Z. Wang, Construction and evaluation of Fe_3O_4-based PLGA nanoparticles carrying rtPA used in the detection of thrombosis and in targeted thrombolysis, ACS Appl. Mater. Interf. 6 (2014) 5566–5576.
[208] F.-M. Gong, Z.-Q. Zhang, X.-D. Chen, L. Zhang, X.-S. Yu, Q.-H. Yang, X.-T. Shuai, B.-L. Liang, D. Cheng, A dual ligand targeted nanoprobe with high MRI sensitivity for diagnosis of breast cancer, Chinese J. Polym. Sci. 32 (2014) 321–332.
[209] Y. Sun, Y. Zheng, H. Ran, Y. Zhou, H. Shen, Y. Chen, H. Chen, T.M. Krupka, A. Li, P. Li, Z. Wang, Z. Wang, Superparamagnetic PLGA-iron oxide microcapsules for dual-modality US/MR imaging and high intensity focused US breast cancer ablation, Biomaterials 33 (2012) 5854–5864.
[210] L.J. Cruz, P.J. Tacken, F. Bonetto, S.I. Buschow, H.J. Croes, M. Wijers, I.J. de Vries, C.G. Figdor, Multimodal imaging of nanovaccine carriers targeted to human dendritic cells, Mol. Pharm. 8 (2011) 520–531.
[211] K.J. Dormer, V. Awasthi, W. Galbraith, R.D. Kopke, K. Chen, R. Wassel, Magnetically-targeted, technetium 99m-labeled nanoparticles to the inner ear, J. Biomed. Nanotechnol. 4 (2008) 174–184.
[212] P. Pouponneau, J.-C. Leroux, S. Martel, Magnetic nanoparticles encapsulated into biodegradable microparticles steered with an upgraded magnetic resonance imaging system for tumor chemoembolization, Biomaterials 30 (2009) 6327–6332.
[213] C. Liao, Q. Sun, B. Liang, J. Shen, X. Shuai, Targeting EGFR-overexpressing tumor cells using Cetuximab-immunomicelles loaded with doxorubicin and superparamagnetic iron oxide, Eur. J. Radiol. 80 (2011) 699–705.
[214] N. Schleich, P. Sibret, P. Danhier, B. Ucakar, S. Laurent, R.N. Muller, C. Jerome, B. Gallez, V. Preat, F. Danhier, Dual anticancer drug/superparamagnetic iron oxide-loaded PLGA-based nanoparticles for cancer therapy and magnetic resonance imaging, Int. J. Pharm. 447 (2013) 94–101.
[215] C. Wang, S. Ravi, G.V. Martinez, V. Chinnasamy, P. Raulji, M. Howell, Y. Davis, J. Mallela, M.S. Seehra, S. Mohapatra, Dual-purpose magnetic micelles for MRI and gene delivery, J. Control. Release 163 (2012) 82–92.
[216] Y. Liu, L. Feng, T. Liu, L. Zhang, Y. Yao, D. Yu, L. Wang, N. Zhang, Multifunctional pH-sensitive polymeric nanoparticles for theranostics evaluated experimentally in cancer, Nanoscale 6 (2014) 3231–3242.
[217] S.L. Li, K.L. Hu, W.P. Cao, Y. Sun, W. Sheng, F. Li, Y. Wu, X.J. Liang, PH-responsive biocompatible fluorescent polymer nanoparticles based on phenylboronic acid for intracellular imaging and drug delivery, Nanoscale 6 (2014) 13701–13709.
[218] T. Fischer, R. Ladurner, A. Gangkofer, T. Mussack, M. Reiser, A. Lienemann, Functional cine MRI of the abdomen for the assessment of implanted synthetic mesh in patients after incisional hernia repair: initial results, Eur. Radiol. 17 (2007) 3123–3129.
[219] B. Porsio, L. Lemaire, S. El Habnouni, V. Darcos, F. Franconi, X. Garric, J. Coudane, B. Nottelet, MRI-visible nanoparticles from hydrophobic gadolinium poly(ε-caprolactone) conjugates, Polymer 56 (2015) 135–140.